

# Chapter 1

## Paleoclimate

Patrick J. Bartlein, Steven W. Hostetler and Jay R. Alder

### 1.1 Introduction

As host to one of the major continental-scale ice sheets, and with considerable spatial variability of climate related to its physiography and location, North America has experienced a wide range of climates over time. The aim of this chapter is to review the history of those climate variations, focusing in particular on the continental-scale climatic variations between the Last Glacial Maximum (LGM, ca. 21,000 years ago or 21 ka) and the present, which were as large in amplitude as any experienced over a similar time span during the past several million years. As background to that discussion, the climatic variations over the Cenozoic (the past 65.5 Myr, or 65.5 Ma to present) that led ultimately to the onset of Northern Hemisphere glaciation at 2.59 Ma will also be discussed. Superimposed on the large-amplitude, broad-scale variations from the LGM to present, are climatic variations on millennial-to-decadal scales, and these will be reviewed in particular for the Holocene (11.7 ka to present) and the past millennium.

#### 1.1.1 The Climate System and Its Controls

The *climate system*, a set of coupled environmental systems, whose controls, interactions, state, and variability can be thought of as the subject matter of *climatology*, can be described by a set of external controls, “fast-response” variables that vary with characteristic time scales of seconds to years, a set of “slow-response variables” with characteristic time scales of variation of years and longer,

---

P. J. Bartlein (✉)  
University of Oregon, Eugene, OR, USA  
e-mail: bartlein@uoregon.edu

S. W. Hostetler · J. R. Alder  
US Geological Survey, Oregon State University, Corvallis, OR, USA

and a third set of environmental subsystems that vary in response to climate (Fig. 1.1; Harrison and Bartlein 2012). The external controls that “force” the climate system include *solar radiation* (insolation), which depends on the output of the sun and the Earth’s orbital variations that govern the latitudinal and seasonal variations of insolation, and *geodynamics* that influence topography and bathymetry of the globe, and the location and variability of volcanism. The slow-response variables of the climate system include such components as the ice sheets, the deep ocean, the thermohaline circulation of the ocean (otherwise known as the global conveyor belt or AMOC, the Atlantic meridional overturning circulation), and the major reservoirs of global biogeochemical cycles (for example, the terrestrial biosphere and trace-gas composition of the atmosphere). Fast-response variables include those components that are often thought of as weather, such as atmospheric circulation and its control of precipitation and surface temperature, but they also include the characteristics of the land-surface, i.e. snow, ice and water, vegetation, variations in biogeochemistry and the surface layer of the ocean.

Also included in the climate system are the major environmental subsystems, such as the surface hydrology, biosphere, and humans. In general, the state of the climate system can be considered to be governed by a hierarchy of controls and responses in which the external controls force the slow-response variations as in, for example, the way that insolation controls global ice volume and ocean temperatures; the slow-response variables, in turn, force the fast response variables as in, for example, the way that the Laurentide Ice Sheet (LIS) controls atmospheric circulation (see following sections). The fast-response variables in turn govern individual environmental subsystems (Fig. 1.1). This hierarchy of control and response is not strictly unidirectional, inasmuch as the “current state” of the ocean and land surface can ultimately feed back to the slow response variables. The specific roles the individual components play in generating climatic variation is strongly dependent on the time and space scales under consideration. For example, on the longest of time spans considered here, the Cenozoic (65 Ma to present), continental-scale glaciation was controlled by the overall state of the climate, in particular global-average temperature. On shorter time scales, such as the Quaternary (2.59 Ma to present) the volume of ice varied with insolation as its “pacemaker”, and the size of the ice sheets can be considered to be a general index of the global climate. On still shorter interannual to decadal time scales, rather than being considered a response variable, the size and shape of the large ice sheets remain constant enough for them to be considered a large-scale control (e.g. of atmospheric circulation). Individual components of the climate system thus may play different roles depending on the time scale and the attendant state of the system—acting as the responses on one time and space scale, but as controls on another. Because, for example, the growth and decay of ice sheets is determined by the balance between accumulation and melting at the surface, those responses lower in the hierarchy, when integrated over time, become the proximate controls of those components higher in the hierarchy of controls and responses.

There are two general approaches for the study of past climate, the reconstruction of past climatic variations from various sources of paleoclimatic evidence,

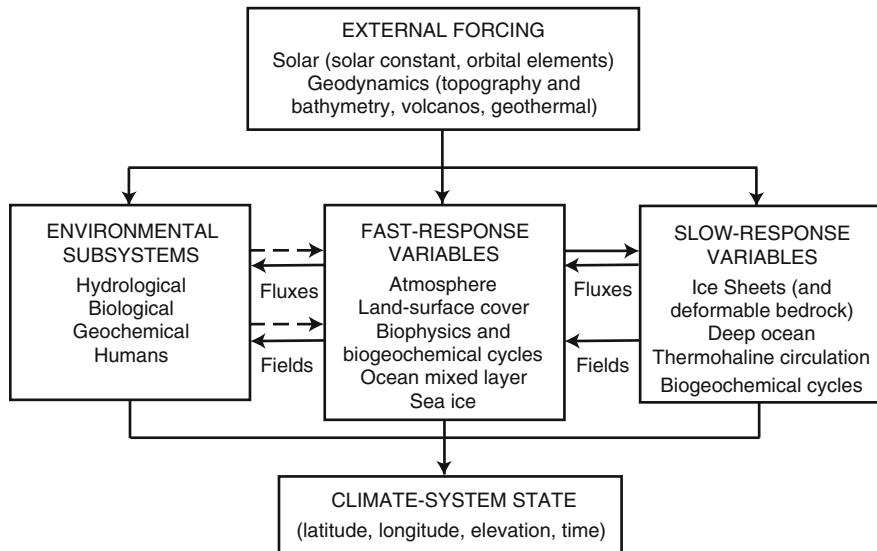


**Fig. 1.1** The climate system (after Saltzman 2002; Harrison and Bartlein 2012)

and the simulation of past climates using a range of different kinds of climate models (Bartlein and Hostetler 2004). The two approaches are complementary: paleoclimatic evidence documents what has happened in the past, but it cannot explain the source or mechanisms that caused the variations without invoking some kind of model, either conceptual, statistical or mechanical, whereas mechanistic models can yield such explanations, but only if the models are known to be correct, and this can be evaluated with paleoclimatic data. At first glance, this relationship may appear circular, but it is in fact iterative, because our current understanding of past climates is used to generate hypotheses that can be tested with models, leading in turn to refinements in our understanding of climate and improvements to the climate models, which allows for the development of further testable hypotheses.

### 1.1.2 Paleoclimate Data Sources

The evidence for past climatic variations is generally provided by environmental subsystems that record the current state of their controls. Paleoclimatic data sources include a range of biological and geochemical indicators retrieved from sediments, as well as direct lines of geomorphic or geological evidence such as the former shorelines of lakes or end moraines of glaciers. The data sources and methods of paleoenvironmental reconstruction are described well in books by Bradley (1999) and Cronin (2010), and are not discussed at length here.

### 1.1.3 Paleoclimate Models

There are several classes of paleoclimate models (Bartlein and Hostetler 2004). These classes include (a) conceptual models that describe the variability of individual components of the climate system as well as the system as a whole, (b) elemental models that mechanistically describe one or more components, but usually in highly generalized ways, and current-generation “coupled” models that describe several or more individual components of the climate system, including (c) general circulation models of the ocean, atmosphere and terrestrial biosphere (OAVGCMs), and (d) Earth System Models of Intermediate Complexity (EMICs) that do the same at generally reduced spatial resolution and with a more stylized representation of some key components than in GCMs (allowing long simulations with many components to be made), and finally (e) the emerging Earth-System Models (ESMs) that aim to include all of the climatically relevant processes and subsystems that comprise the climate system.

In their application to simulate past climatic variation, the models are supplied with a set of “boundary conditions” or the large-scale controls of climate, such as atmospheric composition, insolation, and the topography of the major ice sheets, and then “integrated” (run) to produce a large number of variables that are consistent with the specified boundary conditions. This procedure in effect mimics in the computer the experiments performed by Nature with the real climate system.

Our focus here will be on the results from a fully-coupled ocean–atmosphere general circulation model (OAGCM) GENMOM (Alder et al. 2011), that are pertinent to North America, and provide a sequence of simulations of a variety of climate variables at 3 kyr intervals from the LGM to present. These new simulations update previous simulations that were performed with models in which ocean temperatures were specified (COHMAP Members 1988) or calculated using a “mixed-layer” ocean (Bartlein et al. 1998) and consequently did not adequately represent key paleoclimatic controls such as the reorganization of ocean circulation.

We also use time series of temperature extracted from a “transient” climate simulation conducted with the Community Climate System Model-3 (CCSM3) (Liu et al. 2009) that was run continuously from 22 ka to present, with “realistic” variations in the controls, in particular the fresh-water forcing responsible for the abrupt climate changes during deglaciation (Clark et al. 2012). These time series illustrate seasonal changes in climate over the past 22 kyr, and also show the regional variations in the expression of abrupt climate changes during this interval.

## 1.2 Long-Term Paleoclimatic Variations: Cenozoic Cooling and the Onset of Glaciation

The pronounced glacial-interglacial climate variations of the Quaternary, which have played a prominent role in shaping the landscape of North America (both within and beyond the limits of glaciation), represent the culmination of a long

period of cooling. Although large in amplitude, the long cooling trend and glacial-interglacial variations have superimposed upon them equally significant variations of climate on millennial-to-interannual time scales.

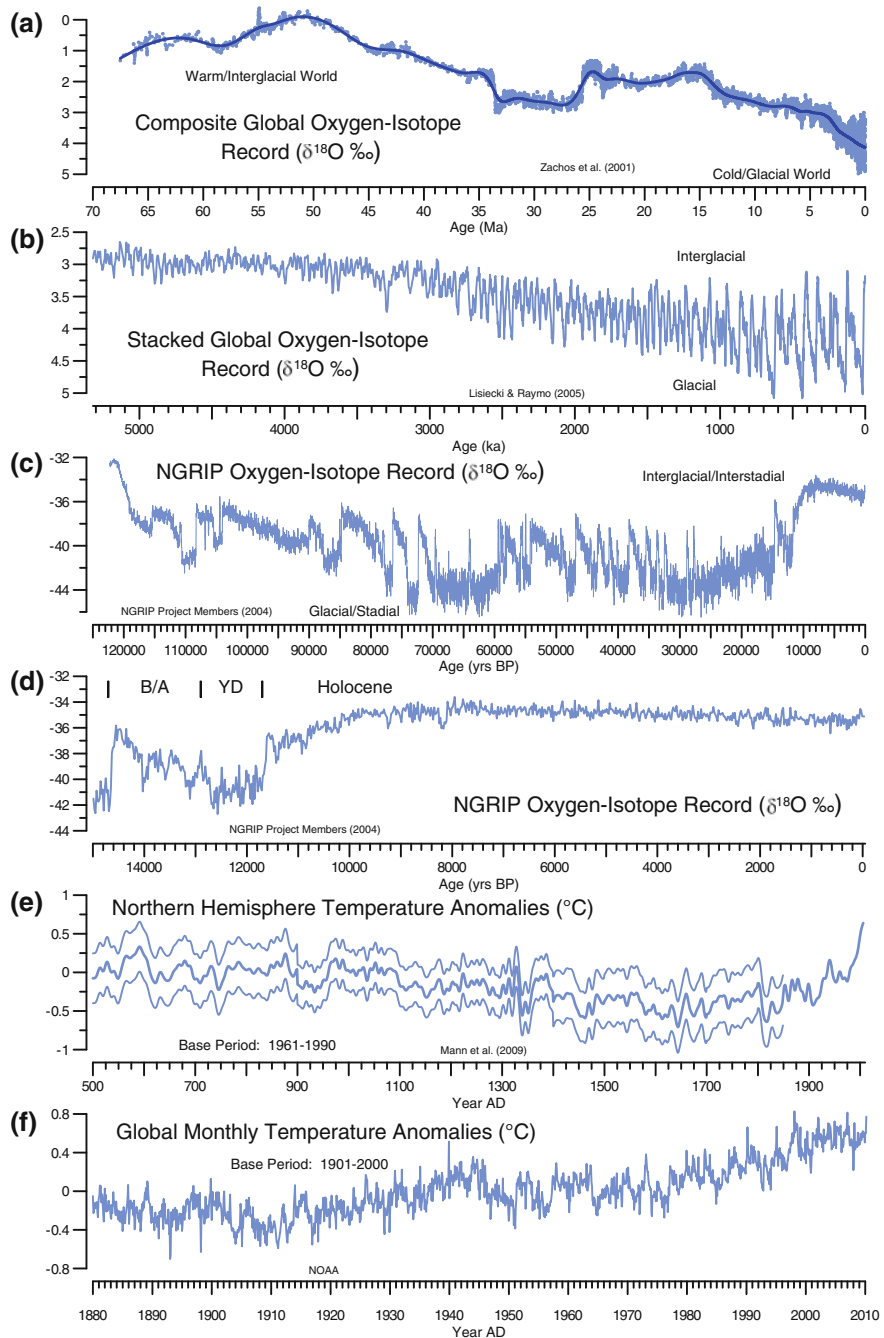
### 1.2.1 A “Powers-of-Ten” Review of Climate Variability

Climate varies continuously, and although the state of the climate tends to remain within well-defined “corridors” over long periods of time, the concept of an “average” climate is an incomplete one—most of the time the climate system is in one state or configuration, and trending toward another. This style of variation can be seen by examining variations of climate on different time scales by the “powers-of-ten” approach (Fig. 1.2). Although the curves described here represent global climate, climatic variations over North America reflect those of globe. The individual records will also show that there is a limit in resolution in any paleoclimatic record that is a joint function of the intrinsic resolution of a record and of the analysis approaches. Most terrestrial and marine records spanning many thousands or millions of years generally cannot be analyzed at, for example, annual or decadal resolutions because sedimentation rates are limiting (one sample may span hundreds to thousands of years) or because analytical issues may arise (short-term variations may be undetectable using common laboratory and analytical procedures). Likewise, high-resolution records are generally short, owing to interventions in the particular observing system (e.g. annual-resolution dendroclimatic records extend only to the life of individual trees or to those of cross-dated groups of trees).

Over the Cenozoic (the past 65.6 Myrs, Fig. 1.2a), the main change in global climate has been a nearly monotonic trend toward cooler conditions, as indexed by oxygen-isotope values in the composite record from marine sediments shown in the Figure (Zachos et al. 2001). Other modes of climatic variability are evident in the records (Bartlein 1997) including an abrupt (at the time scales described by the curve) event or “spike” in temperatures around 53 Ma, known as the Paleocene-Eocene Thermal Maximum (PETM), several downward “steps” in temperature, such as those around 35 Ma when Antarctica became glaciated, and in the past 5 Myrs accompanying the closure of the Central American seaway.

When that 5 Myr interval is expanded in a “stacked” or composite oxygen-isotope record, again from marine sediments (Fig. 1.2b), the nature of the variability that is superimposed on the Cenozoic trend is revealed (Lisiecki and Raymo 2005), and what appears as a step in the Cenozoic time series is a trend over this 5 Myr interval. As will be described further below, this variability is largely an expression of the response of global climate to orbitally driven variations in insolation. Changes in the variability of climate can also be noted, particularly around 2.5 Ma, and again at 1 Ma. The persistence of these changes in variability demonstrates that the climate of any interval cannot be simply described by only its long-term mean.

Figure 1.2c shows the oxygen-isotope record from the NGRIP (North Greenland Ice Core Project Members 2004) ice core, and expands the last 100 kyr of the



◀ **Fig. 1.2** Powers-of-ten depiction of climate variations over the past 65.5 Myrs. (Zachos et al. 2001; Lisiecki and Raymo 2005; North Greenland Ice Core Project Members 2004; Mann et al. 2009; Mann et al. 2008), also (f) NOAA (<http://lwf.ncdc.noaa.gov/sotc/>) The oxygen-isotope curves are plotted such that colder conditions are represented by the low values of each curve and warmer conditions by the high values. **a** Composite Global Oxygen-Isotope Record ( $\delta^{18}\text{O} \text{ ‰}$ ), **b** Stacked Global Oxygen-Isotope Record ( $\delta^{18}\text{O} \text{ ‰}$ ), **c** NGRIP Oxygen-Isotope Record ( $\delta^{18}\text{O} \text{ ‰}$ ), **d** NGRIP Oxygen-Isotope Record ( $\delta^{18}\text{O} \text{ ‰}$ ), **e** Northern Hemisphere Temperature Anomalies and Reconstruction Uncertainties (°C), **f** Global Monthly Temperature Anomalies (°C)

stacked marine record. In addition to the “saw-tooth” pattern of the last glacial-interglacial cycle, the ice-core record reveals the frequent abrupt changes of climate known as the Dansgaard-Oeschger “cycles”. (Although repeated, these variations are clearly not truly periodic or even quasi-periodic and so are not cyclical). Figure 1.2d shows an expanded plot of the last 15 kyrs of the NGRIP record, and illustrates the most recent large-amplitude variation of the longer record, and the relatively (in this record) lower amplitude variations of climate in Greenland over the Holocene (the past 11.7 kyr). The cool interval between 12.9 and 11.7 ka, known as the Younger Dryas climate reversal, will be discussed further below. Although the Holocene seems far less variable than the earlier intervals in the NGRIP record, there are still trends and abrupt “events”, such as that around 8.2 ka, evident in the record.

Reconstructed Northern Hemisphere temperatures (Fig. 1.2e), (Mann et al. 2009; Mann et al. 2008) exhibit a general high-latitude cooling trend over the past millennium that is present in other records (Kaufman et al. 2009). There is a clear reversal of that trend in the past 200 years, with the commencement of anthropogenic warming (IPCC 2007). Relative to the past 1000 years, and to the Holocene as a whole, this reversal appears more event-like than a change in trend. Global-average monthly temperatures from observations (Fig. 1.2f) show the anthropogenic trend, and also reveal the magnitude of interannual variations of climate, which are larger for individual regions and locations than those in this globally averaged record.

When the individual records are compared with one another, two basic conclusions emerge: (1) the higher frequency variations evident in the shorter records (e.g. Fig. 1.2e, f) are also present over longer time spans, but the resolution and the nature of the longer-term records complicate their detection and (2) higher-frequency variations are contingent on the long-term changes in the climate system that are represented by the longer term, lower-frequency records.

### **1.2.2 The Last 3 Million Years and the Onset of Glaciation**

The onset of Northern Hemisphere glaciation around 2.65 Ma was a major transition of climate that marks both the beginning of the Quaternary and the beginning of the repeated climate variations that have shaped both the landscapes and biota of North America (Lisiecki and Raymo 2005), Fig. 1.2b. Although there were likely regional areas of glaciation in North America prior to this time that also

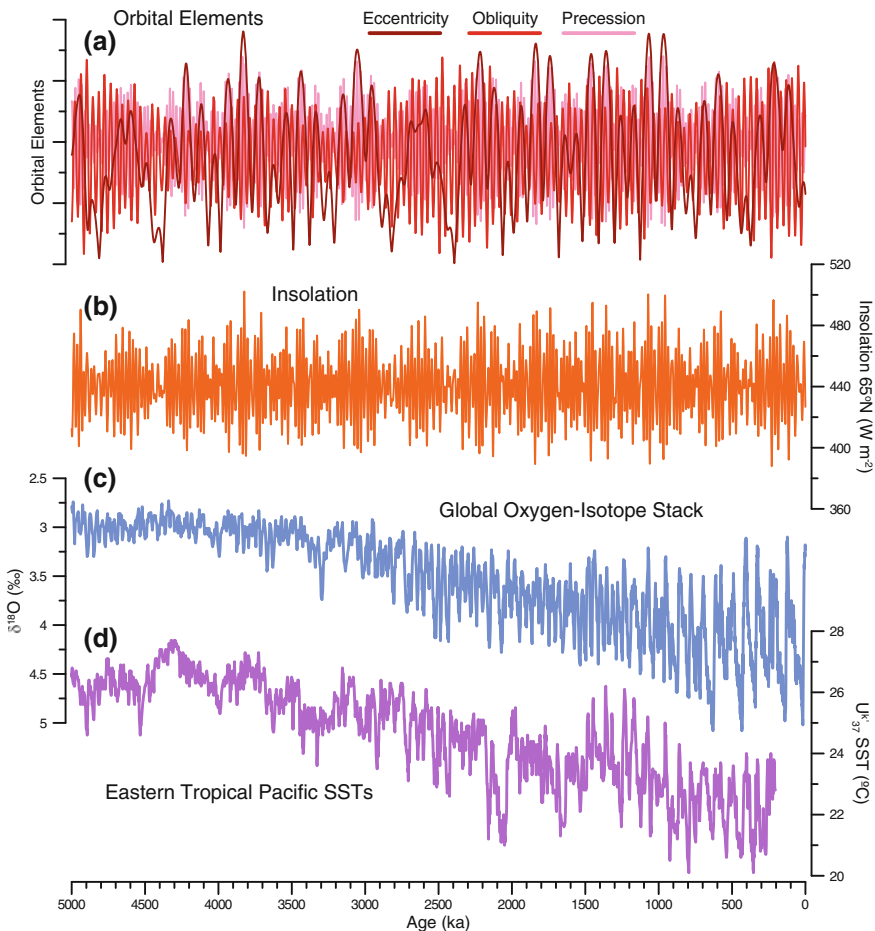


**Fig. 1.3** The last 5 million years. **a** orbital elements (Berger and Loutre 1991); **b** July insolation at 65 N; **c** global oxygen-isotope record stack (Lisiecki and Raymo 2005), **d** eastern tropical Pacific alkenone SSTs (Lawrence et al. 2006). The two marine records show the trend toward cooler conditions, the steeper transition around 2.5 Ma signaling the onset of Northern Hemisphere glaciation, as well as the change in variability of the series. The insolation record (and the orbital elements that determine it), does not show the transitions or trends in the observations, but clearly shows its role in pacing the climatic variations

varied in concert with insolation (see Cronin (2010), Chap. 4 for review), after 2.65 Ma there were repeated large-scale glaciations of North America, varying first primarily on the 41 kyr time scale of obliquity (Fig. 1.3) from 2.65 Ma to around 1 Ma, and thereafter on the 100 kyr cycle of eccentricity (See Harrison and Bartlein (2012) for a discussion of orbital time-scale variations in insolation, including the variations in month and season lengths related to variations in Earth's orbit.).

Global and regional climates (Fig. 1.3c, d) both show substantial variation on the timescales of the orbital elements, but the onset of glaciation is difficult to attribute to

a particular pattern of insolation variations, and instead is likely related to progressive changes in other controls of climate, in particular the long-term decrease in atmospheric CO<sub>2</sub> levels during the Cenozoic (Beerling and Royer 2011), and to geodynamic variations, such as the closure of the “Panamanian Straits” (Haug et al. 2005; Haug and Tiedemann 1998). The general decrease in CO<sub>2</sub> levels and associated change in radiative forcing favors glaciation through direct and indirect influence on surface temperatures. Changes in ocean circulation accompanying the uplift of the Isthmus of Panama, which reduced the amount of heat transferred from the tropical Atlantic to the Pacific, supported glaciation in a counter-intuitive way—a warmer tropical Atlantic would have resulted in greater transport of warm water and water vapor to the circum-North Atlantic region, thereby increasing snowfall in the regions where the large Northern Hemisphere ice sheets develop.

That insolation variations pace the paleoclimatic variations on orbital time scales is clear; however, the specific mechanisms that implement that pacing remain unknown, despite over a century-and-a-half of research, except that it is evident that the climate system must include mechanisms for amplifying insolation and other forcing (Harrison and Bartlein 2012; Kohler et al. 2010), and for generating the characteristic 41 and 100 kyr variations of ice volume (Ruddiman 2006; Abe-Ouchi et al. 2013). A succinct review of some of the many hypotheses that have been advanced is provide by Table 5.1 in Cronin (2010).

The influence of insolation variations is not limited to the regular pacing of the growth and decay of ice sheets; the variations also force orbital-time scale variations of land–ocean temperature contrast, and hence modulate monsoonal circulation systems and associated mid-continental moisture levels. Even in the absence of large ice sheets, climatic variations have occurred on orbital timescales, and considering that the monsoon regions encompass global areas more extensive than glaciated regions, orbital time-scale variations of climate independent of glaciation should be considered the principle mode of climate variability on times scales from thousands to millions of years. These non-glacial, insolation-driven variations are easily illustrated using the Holocene record of climate change of North America, which will be discussed later.

An important perspective provided by the record of climatic variations over the past few million years is that climate changes are both progressive and recurrent. Over this interval, the long-term mean state exhibits gradual cooling together with an increase in amplitude of the variation, with warm, interglacial intervals cooling less than the cold, glacial intervals. On top of these progressive changes are repeated and rapid (on this time scale) glacial/interglacial variations. Although recurrent, the climate variations within a given cycle are not identical with those of other cycles (nor in detail are the driving insolation variations), so while the individual cycles broadly resemble one another, they are not exact replications. One consequence of the recurrent nature of the orbital variations is that the terrestrial and marine biospheres (including both plants and animals) must have evolved in way that lets them respond to the high-amplitude orbital variations with only occasional extinctions (Bartlein and Prentice 1989; Bennett 1997).

### 1.3 The Last Glacial Cycle: Orbital Time-Scale Variations and Abrupt Climate Change

The last glacial cycle spans the interval from around 130 ka to present, and paleoclimatic records show orbital time-scale variations and abrupt variations on shorter time scales (Fig. 1.4). Figure 1.4 shows a selection of long paleoclimatic time series from around North America, as well as January and July insolation anomalies (differences from present) at 45°N (Berger 1978), and the SPECMAP (Imbrie et al. 1992) stacked-and-smoothed record of marine oxygen-isotopic variations as an index of global ice volume (plotted on an inverse scale, with warm, less-ice conditions at the top, and cold, more-ice conditions at the bottom).

#### 1.3.1 The Previous Interglacial to the Holocene

The previous interglacial period in North America, known as the *Sangamon*, and equivalent to the European *Eemian* (both outmoded, but frequently used terms arising from the now obsolete idea that there were four glacial stages, separated by interglacials, on both continents) is equivalent to marine oxygen-isotopic stage 5e (MIS-5e, 128–122 ka). The July (boreal summer) insolation and global ice-volume records illustrate two of the major controls of regional climates over the past glacial-interglacial cycle (see the next section) and they serve as well as a general index of global climate. Northern Hemisphere summers during the previous interglacial were likely warmer than those of the present interglacial (the Holocene, i.e. 11.7 ka to present), owing to the greater northern summer insolation then, as well as sufficiently reduced global ice volume (relative to the current interglacial) to create global sea levels that were 6 m higher than present (Overpeck et al. 2006; Anderson et al. 2006). From the previous interglacial to the Last Glacial Maximum (LGM), (26.5 to 19 ka; Clark et al. 2009) global climate cooled in stages, with increases in ice corresponding to falling levels of July insolation, and slight decreases accompanying increases in July insolation.

Paleoclimatic records from around North America, including the NGRIP ice-core record from Greenland (North Greenland Ice Core Project Members 2004), North Atlantic (Wolff et al. 2012) and Caribbean (Schmidt et al. 2004) sea-surface temperature (SST) records, Santa Barbara Basin oxygen-isotope and marine taxon records (Hendy and Kennett 2003; Hendy et al. 2002) and pollen records from Utah (Jiménez-Moreno et al. 2008) and Florida (Donders et al. 2011a; Grimm et al. 1993) are all either dominated by or reflect to some extent the general trends of insolation and ice volume, a pattern that is typical of paleoenvironmental records that extend over this interval (Webb and Bartlein 1992; see also Whitlock and Bartlein 1997).

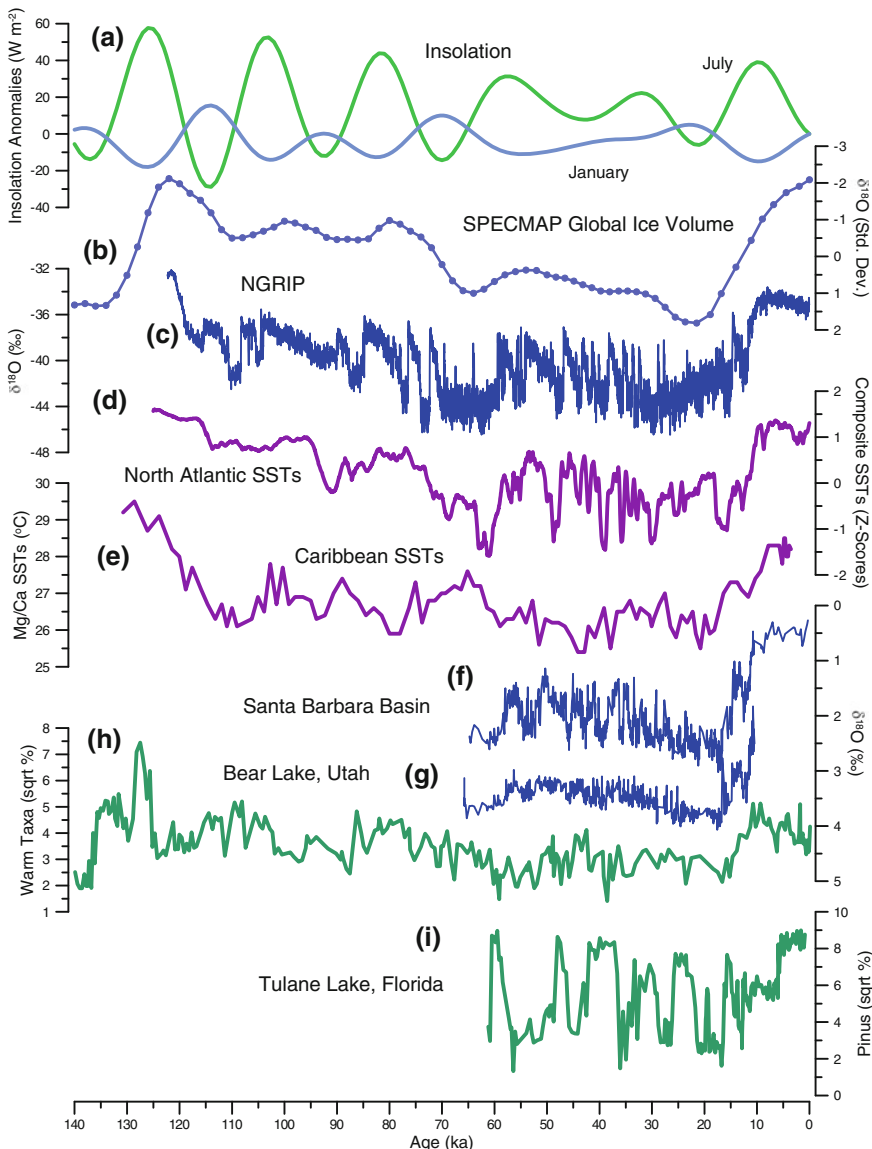


**Fig. 1.4** Representative time series that span the past 130 kyr—the last glacial/interglacial cycle. **a** insolation in January and July at 45°N (Berger and Loutre 1991); **b** global ice volume (Martinson et al. 1987); **c** NGRIP oxygen-isotope values (North Greenland Ice Core Project Members 2004); **d** a stack of North Atlantic SST records (Harrison et al., in prep); **e** Caribbean SSTs (Schmidt et al. 2004); **f**, **g** Santa Barbara basin oxygen-isotope values (Hendy and Kennett 2003; Hendy et al. 2002); **h** Bear Lake, Utah pollen data (Jimenez-Moreno et al. 2007); **i** Tulane Lake, Florida pollen data (Donders et al. 2011b)

### 1.3.2 Abrupt Climate Changes

The most striking features of the individual records shown in Fig. 1.4, however, are the many abrupt changes of climate with amplitudes that often exceed more than half of the total range of variation between full glacial and interglacial conditions. This is best illustrated by the NGRIP oxygen-isotope record, which approaches annual resolution throughout (North Greenland Ice Core Project Members 2004). During the interval from 80 ka to around 15 ka, around 25 individual fluctuations, known as Dansgaard–Oeschger (D-O) “cycles” occurred (although the individual fluctuations vary considerably in duration and are therefore not really cyclical; Sanchez Goñi and Harrison 2010). The origin of these fluctuations is likely related to variations in AMOC, and its influence on ocean heat transport, initiated by freshwater discharges to the North Atlantic. However, like the orbital variations, the specific mechanisms involved in the response have yet to be fully articulated (Wolff et al. 2010). The individual fluctuations have a characteristic sawtooth-curve shape, with abrupt warming steps, followed by gradual cooling over varying time spans (Fig. 1.4).

Variations in terrestrial (Jiménez-Moreno et al. 2010) and marine (e.g. Hendy and Kennett 2003; Hendy et al. 2002) conditions are evident around North America, and their expression in paleo records depends chiefly on the resolution of the records—those that have sampling resolutions of a few decades or less typically show these abrupt changes, although there are also some spatial variations in the expression of the fluctuations that will be illustrated below.

The most recent abrupt change—and the last during glacial times—is the Younger Dryas climate reversal (YDCR) that is characterized by a cooling trend beginning around 14.5 ka with more rapid intervals of cooling around 13.5 and 12.9 ka, and was terminated by abrupt warming around 11.7 ka (Alley et al. 2003; Steffensen et al. 2008). Like the earlier D-O cycles, the YDCR is expressed in terrestrial records from North America (Shuman et al. 2002; Shuman 2012) and also like the earlier fluctuations, the genesis of the YDCR has been related to the shutdown of the AMOC, in particular by the rapid drainage of Lake Agassiz and other proglacial lakes (in the midcontinent at the southern edge of the ice sheet) and the consequent flow of fresh water to the Atlantic (Carlson et al. 2007; Liu et al. 2012). Alternative explanations for the YDCR are that it was forced by outflow of the proglacial lakes along the LIS into the Arctic Ocean by way of the Yukon (Condron and Winsor 2012; Teller 2012), which is still consistent with the idea of an AMOC shutdown, or that it resulted in some way from the impact of an extraterrestrial object (Firestone et al. 2007).

Many of the individual lines of evidence claimed to support this latter explanation have been difficult to reproduce (Pinter et al. 2011; Boslough et al. 2012) or have much simpler alternative explanations (Marlon et al. 2009; Carlson 2010) but perhaps the main challenge for the impact mechanism is that it is simply unnecessary—abrupt climate changes like the YDCR occur throughout the record, and large climate reversals at the beginning of interglacial intervals are features of

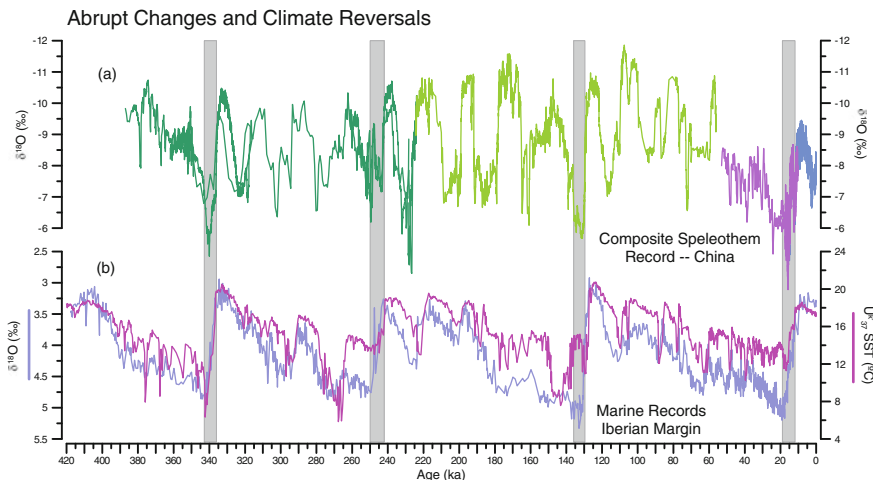


**Fig. 1.5** Abrupt climate changes during the past four glacial/interglacial cycles. **a** composite speleothem oxygen-isotope record from China (Cheng et al. 2009); **b** marine records from the Iberian Margin (North Atlantic; Martrat et al. 2007). The records show that the abrupt climate changes like the Younger Dryas Climate Reversal (YDCR) that occurred during the last glacial/transition are ubiquitous in previous deglaciations, and therefore do not require special explanations

earlier deglaciations. Figure 1.5 shows two records of sufficient length to span several glacial/interglacial cycles and sufficient resolution to record abrupt climate changes: a composite speleothem oxygen-isotope record from China (Cheng et al. 2009), and a temperature and oxygen-isotope record from the North Atlantic (Martrat et al. 2007). Although not specific to North America, there is nothing to suggest that the climatic variations shown in these records are regionally unique or idiosyncratic (compare Figs. 1.4 and 1.5), and it is likely that abrupt climate changes like those in China and the western Atlantic also occurred during earlier glacial-interglacial variations in North America. These records clearly show that abrupt climate changes during the last glacial/interglacial cycle are not unprecedented, and that YDCR-like fluctuations often occur at glacial terminations (Broecker et al. 2010), eliminating the need for an exceptional or special explanation for the YDCR.

## 1.4 The Last Glacial Maximum to Present

Between the Last Glacial Maximum (LGM) and present, the climate system as a whole, and North America in particular experienced a range of climates as large as any that occurred during the past 2.65 Myr. The scope of these variations and the changes in the large-scale controls of climate that generated them provide a set of

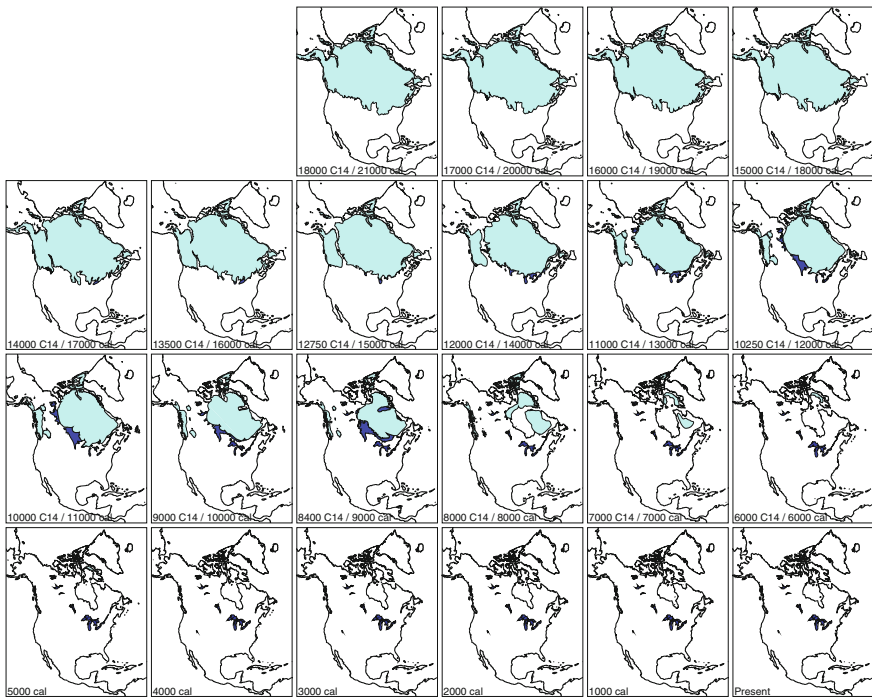


**Fig. 1.6** Deglaciation of North America (after Dyke 2004), with continental outlines inferred from data in Peltier (2004)

“natural experiments” that can be exploited through the comparison of climate-model simulations and paleoclimatic data syntheses. Such “data-model” comparisons can lead to mechanistic explanations for patterns recorded by the data and can also be used to test the climate models. Although such an approach may seem to be circular it is actually iterative, with one generation of data-model comparisons leading to refinements of the hypotheses and the overall experimental design and to the identification of particular features of climate that are well or poorly simulated by the models (Harrison and Bartlein 2012; Harrison et al. 2013).

#### 1.4.1 Boundary Condition Changes Over the Past 22 kyr

The most obvious control of regional climate changes in North America since the LGM is the LIS (Fig. 1.6). At 21 ka, the ice sheet stretched from the Aleutians to southeastern Canada, and extended into the northern tier of states south of the U.S./Canada border (Dyke 2004), and at the same time, global sea level was ~120 m lower than present, exposing the continental shelves in general, and the Beringian land bridge in particular. As the ice sheet retreated over time, large fresh-water

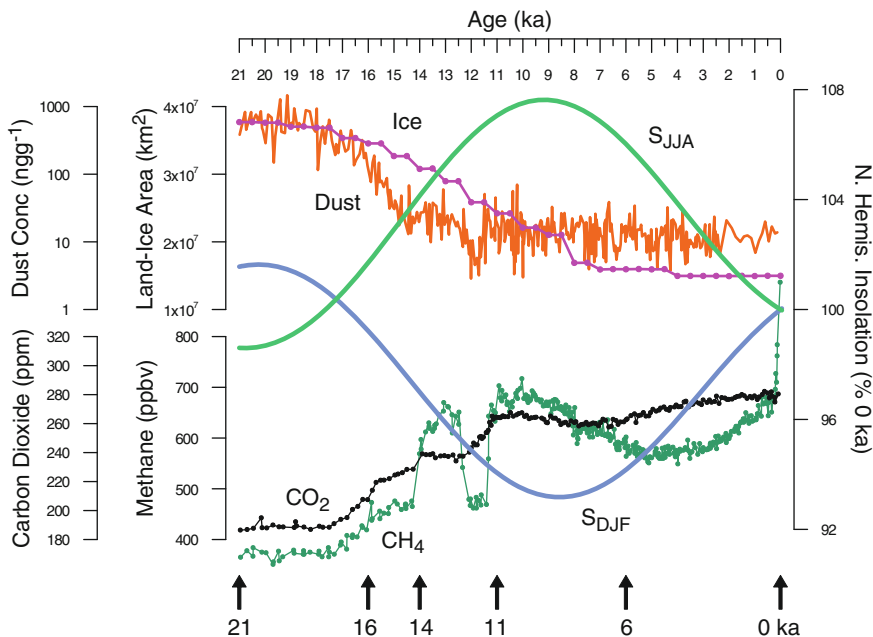


**Fig. 1.7** Boundary conditions for climate-model simulations from the LGM to present (redrawn from Harrison and Bartlein 2012)

(proglacial) lakes formed along the southern margin, where Lake Agassiz attained its maximum size between 12 and 9 ka. By 8 ka, the LIS had disintegrated enough to open the present-day Hudson Bay, and the last remnants of ice (excluding present-day ice on Baffin Island and Greenland) melted just after 6 ka.

On longer (orbital) time scales, the volume and area of the ice sheets can be regarded as “dependent” or internal variables in the climate system. On shorter time scales, ice sheets change slowly enough to be considered as an external control of climate, in much the same way that Antarctica controls Southern Hemisphere climate today. Concentrations of GHGs and aerosols in the atmosphere, like the ice sheets, changed slowly enough on the time span of the last 22 ka so that they can also be regarded as controls as opposed to responses, (Fig. 1.7). The one major control of climate that is truly external over all time-scales is the latitudinal and seasonal distribution of insolation. Over the past 21 kyr, summer insolation in the Northern Hemisphere gradually increased as a consequence of the shift of perihelion into the northern summer (a consequence of the variations in precession), and the greater obliquity then. Summer insolation peaked around 10 ka and decreased thereafter toward the present day. Winter insolation showed the opposite behavior over the interval from 21 ka to present.

Together, the changing boundary conditions provide a set of somewhat idealized experiments in which some controls differ from present while others are nearly the same as today (Fig. 1.7). For example, around the time of the LGM

(e.g. 21 ka), the latitudinal and seasonal distribution of insolation was much the same as at present while “glacial” boundary conditions were at extreme levels, with large ice sheets, low sea levels, low GHGs and high aerosol concentrations. In contrast, at 6 ka, the ice sheets were gone, GHGs and aerosols were near their pre-industrial values, but there was still greater insolation in summer, and less in winter than present. These two times, 21 and 6 ka, are frequently simulated in experiments with climate models, owing to the relative simplicity of the differences in the boundary conditions from those of the present day (Braconnot et al. 2012).

### **1.4.2 Spatial Variations in Simulated Climates, 21 ka to Present**

Several studies have examined sequences of global climate-model simulations and their implications for the LGM-to-present history of climate changes in North America that have used progressively more comprehensive versions of climate models and syntheses of paleo data. These studies focused on simulations using early-generation atmospheric general circulation models (AGCMs) with prescribed sea-surface temperatures, and “perpetual” January and July forcing (e.g., Webb et al. 1987; Barnosky et al. 1987; Webb et al. 1993; Thompson et al. 1993), and later generation AGCMs with mixed-layer oceans (e.g., Bartlein et al. 1998; Webb et al. 1998). Here we use a fully coupled Atmosphere–Ocean General Circulation Model (AOGCM, Alder et al. 2011), that was employed to complete a set of 700-yr “time-segment” simulations at 3 kyr intervals from 21 ka to present (Alder and Hostetler In review). We will compare these simulations briefly with data-based climate reconstructions from terrestrial pollen evidence for the LGM (21 ka) and mid Holocene (6 ka). We also use results from a “transient” (continuous in time) simulation (Liu et al. 2009) to examine the temporal sequence of variations in different regions from 22 ka to the present.

The simulated paleoclimates are shown as climatological differences (also referred to as “anomalies”) between the long-term means of the last 200 years of a given paleo simulation and the pre-industrial “control” simulation, for January and July. For reference, the control values are shown on each Figure. For surface and upper-level winds “anomalous components” of the flow are shown, because these more readily illustrate the change in circulation mechanism than would simply plotting long-term average winds. Anomalous components represent the *difference* in wind speed and direction between a paleo simulation and present, as opposed to the prevailing winds at a particular time. In general, at locations where winds are on average westerly today (i.e. west to east), stronger westerly winds in a paleo simulation will appear as a longer (than for the present day) eastward-pointing vector, whereas weaker-than-present westerly winds in the paleo simulation will appear as a shorter eastward or westward-pointing vector. For any given location, the wind vector anomalies should be compared to the control climatologies.

The specific mechanisms that underlie the sequence of climate changes can be inferred by examining the impact that variations in insolation, GHGs, and the nature of the land surface have on the surface energy balance and, consequently, temperature. Large-scale temperature gradients (and the physical dimensions of the ice sheets) determine the patterns of atmospheric circulation, and hence its role in moisture advection and the distribution of vertical-velocity anomalies (i.e. large-scale uplift and subsidence), which jointly govern precipitation. Precipitation and evapotranspiration, which are constrained by both moisture and energy availability, in turn govern soil moisture. Energy, temperature and moisture variations are ultimately registered by the kinds of environmental processes that are recorded by paleoclimatic data.

### ***1.4.3 Insolation, Net Radiation and Temperature***

Insolation (solar radiation at the top of the atmosphere) is a calculable function of latitude, time of year, and date (Berger 1978). Figure 1.8 shows the smooth variation of insolation over time, and the general pattern of increasing seasonality from the LGM to the early Holocene, and then decreasing seasonality toward present. There are some interesting features superimposed on this overall trend. January insolation anomalies (expressed as absolute values) are muted at high latitudes, owing to the low inputs there, and they increase in magnitude toward the equator. July anomalies reach their greatest amplitudes at high latitudes in the early Holocene and decrease thereafter. These trends combine to produce annual anomalies between 12 and 9 ka (not shown) that are negative equatorward of 45° (in both hemispheres) and positive poleward of 45°, as a consequence of the variations in obliquity, with the Northern Hemisphere high-latitude positive anomalies in summer reinforced by the occurrence of perihelion in summer (Fig. 1.7).

The surface energy balance can be written as:

$$K\downarrow - K\uparrow + L\downarrow - L\uparrow - Q_E - Q_H - \Delta Q_S = 0$$

where  $K\downarrow$  is the incoming (atmosphere to surface) and  $K\uparrow$  the outgoing (surface-to-atmosphere) shortwave (solar) radiation, and  $L\downarrow$  and  $L\uparrow$  are the incoming and outgoing longwave (atmospheric and terrestrial) radiation. Incoming shortwave radiation is a function of insolation, clouds and aerosols, and outgoing shortwave radiation is a function of the albedo of the surface. Incoming longwave radiation is a function of atmospheric temperature, clouds, water vapor and other GHGs, and outgoing longwave radiation is a function of surface temperature.  $Q_E$  is the flux of latent heat and  $Q_H$  the flux of sensible heat from the surface, and  $\Delta Q_S$  is the change in heat storage in the substrate (land or water).

Net radiation at the surface (Fig. 1.9) is the sum of the incoming and outgoing radiative components:

$$Q_{net} = K\downarrow - K\uparrow + L\downarrow - L\uparrow,$$

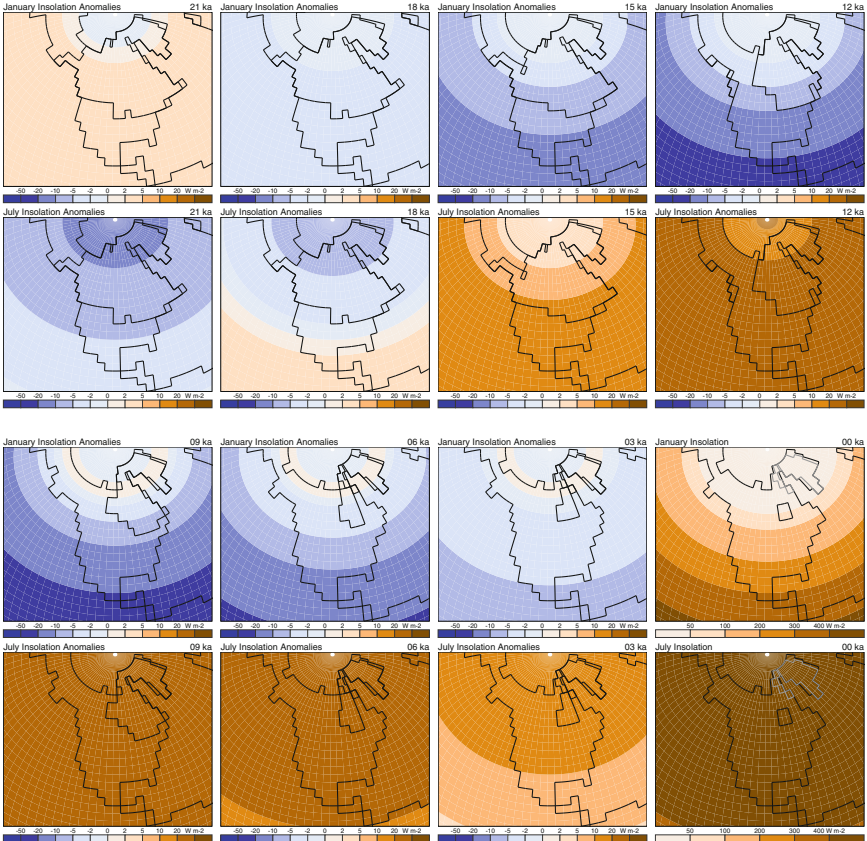


**Fig. 1.8** Top-of-the-atmosphere (TOA) insolation, 21 ka to present (0 ka), from GENMOM, a coupled-ocean atmosphere climate model (OAGCM; Alder et al. 2011; Alder and Hostetler in review). The simulated present-day values in January and July are shown in the last column of the bottom two rows. All other maps are (paleo) experiment minus (present-day) control anomalies, or differences in long-term means. The anomaly patterns are identical at all longitudes, for any particular latitude or season or time

and can be thought of as being disposed of through evapotranspiration and heating the air above the surface or substrate below the surface, i.e.

$$Q_{net} = Q_E + Q_H + \Delta Q_S$$

Net radiation has a strong latitudinal gradient (higher at low latitudes than high), and a high-amplitude annual cycle.

Net radiation anomalies are generally negative in January throughout the sequence of simulations, reflecting the general trends in winter insolation. Some exceptions can be noted, such as in Beringia (the region surrounding the Bering Strait, the Chukchi Sea, and the Bering Sea) from 21 to 9 ka, where the advection of warm air masses from lower latitudes (see below) results in increased net

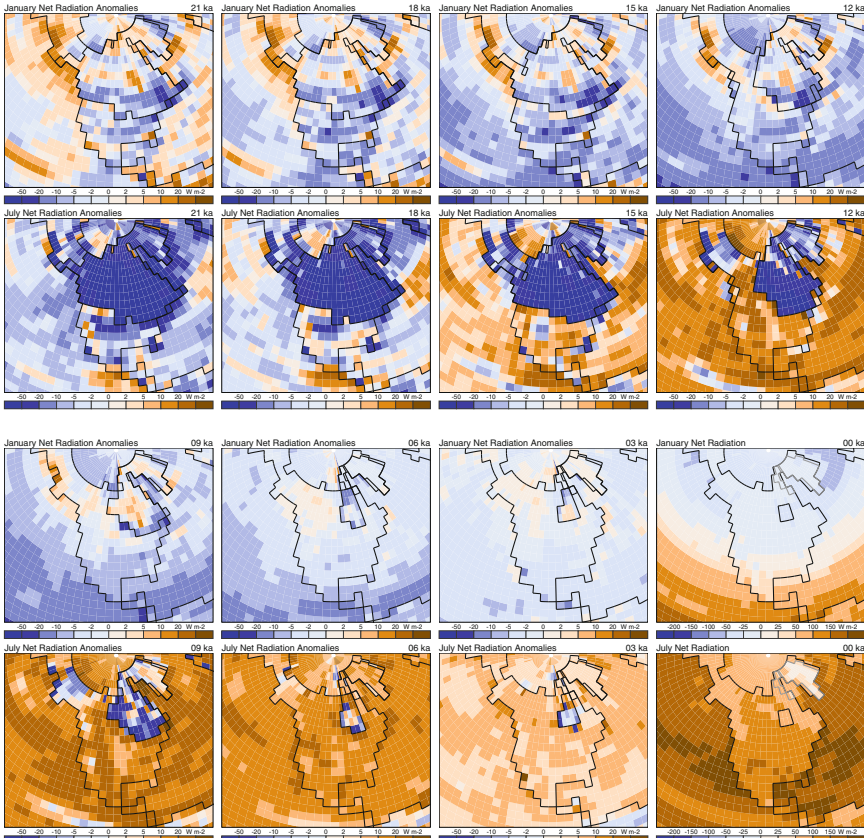


**Fig. 1.9** As in Fig. 1.8, except for net radiation, the sum of net shortwave and longwave radiation at the surface. Note the effect of the high albedo of the ice sheets on July values. January values are not similarly affected, because the regions occupied by the ice sheets are snow covered in winter at present

longwave radiation. Net radiation anomalies in July also track the general trend in summer insolation anomalies, with the important exception of the strongly negative values over the ice sheets, owing to the high albedo of the ice. Because the surface at high latitudes is snow covered in winter at present, large albedo-related net radiation anomalies do not occur in the January simulations.

Simulated 2 m air temperatures (Fig. 1.10) are generally colder than present at 21 and 18 ka, except in Beringia, where southerly winds induced by the influence of the large ice sheet advect air that is warmer at a particular latitude than in adjacent areas. This North Pacific/Beringia “warm-anomaly” is a robust feature of both individual LGM simulations and ensemble averages of LGM simulations (Izumi et al. 2013). Simulated January temperatures at 15 ka resemble those of 21 and 18 ka, while simulated 15 ka July temperatures begin to show the effect of the increasing summer insolation in regions distant from the ice sheet. January

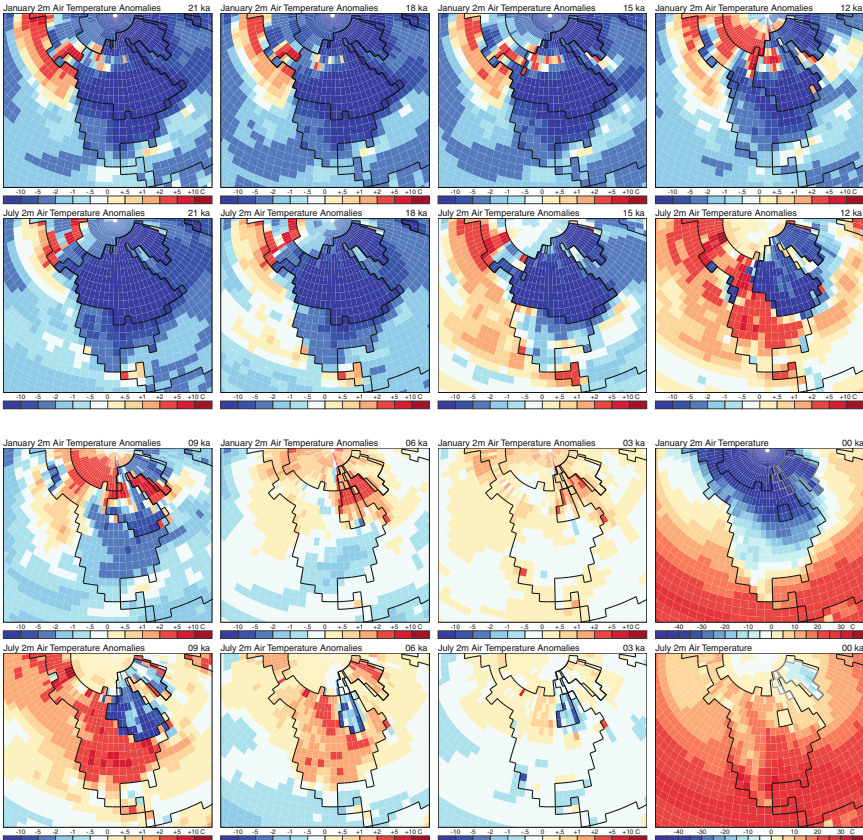


**Fig. 1.10** As in Fig. 1.8, except for near-surface (2 m) air temperature

temperatures at 12 ka remain colder than the present-day, in response to the lower-than-present winter insolation then, but with the important exception of Beringia where the higher-than-present temperatures continue from earlier, and over the Arctic Ocean, where the greater-than-present summer insolation results in the later formation of seasonal sea ice (Figure not shown).

July temperatures increase everywhere (except over the ice sheet itself) at 12 ka in response to the greater-than-present July insolation. This pattern of increased seasonality is amplified further in the 9 ka simulations, when July temperatures are greater than present nearly everywhere except over the residual ice sheet in eastern Canada. From 9 ka to present, July temperatures generally decrease while January temperatures increase, again reflecting changes in insolation. The sequence of simulations also show some temperature patterns that are consistent across climate models and simulations at particular times (Izumi et al. 2013). These include greater cooling over the land than over the ocean at the LGM (and greater warming over the land than over the oceans after the LGM), greater cooling at high latitudes

than at low latitudes at the LGM, and, despite the similarity in the seasonal variations of insolation at the LGM and present, differences in the seasonality of temperature, with lower values over the ice sheet at the LGM and higher values in adjacent regions. As will be discussed further below, although temperature generally increases between the LGM and present day, there are substantial regional and seasonal variations in that overall trend that would yield a rich variety of deglacial temperature histories across the continent.

Near-surface (i.e. reference or anemometer height, usually 2 m) air temperatures are controlled by both the local surface energy balance and the advection of relatively warmer or colder air masses into a region. Comparison of the net radiation anomalies (Fig. 1.9) and temperature anomalies (Fig. 1.10) allows these two controls to be qualitatively separated: similarity in anomaly patterns generally points to an energy-balance control (e.g., over the ice sheet), while divergence generally points to advection of air from adjacent regions as the control (e.g., Beringia from 21 to 12 ka). The distinction between energy-balance and circulation controls is important for understanding the mechanisms through which changes in global-scale controls are registered in individual regions.

#### ***1.4.4 Upper-Level and Surface Atmospheric Circulation***

Upper-level winds (Fig. 1.11) show the response of atmospheric circulation to the joint effect of varying hemispheric temperatures, regional temperature gradients, and the presence of the LIS, which acts as a topographic perturbation in the generally westerly flow. The concentric patterns of slower (pink) and faster (blue) wind speeds, particularly in January from 21 through 12 ka, reveal a pronounced southward shift in the band of fastest westerlies (i.e., the jet stream) relative to their present-day position. The slower-than-present westerly winds at the latitudes where the fastest westerlies prevail today (Canada and the northern U.S.) can be seen in the westward-pointing vectors, particularly in January. The eastward-pointing vector winds in the band of faster winds south of the band of weaker westerlies indicate that onshore flow over the southwestern part of the continent was stronger in the simulations between 21 and 12 ka than in later time periods. Even in the absence of the ice sheet, a southward shift in the westerlies during glacial times is dynamically consistent with the steeper latitudinal temperature gradients during glacial times (much as the westerlies shift equatorward in the winter hemisphere at present).

Close inspection of the anomalous flow-component vectors and comparison with the present day long-term mean patterns shows that in addition to the equatorward displacement of the band of fastest westerlies, there is a tendency for a split in the upper-level flow, with a second branch of the jet stream crossing the continent poleward of the ice sheet. This split, which is caused by orographic lifting and blocking, is particularly evident in July at 21 and 18 ka. The “split jet” is another feature that can be frequently observed in climate-model simulations,

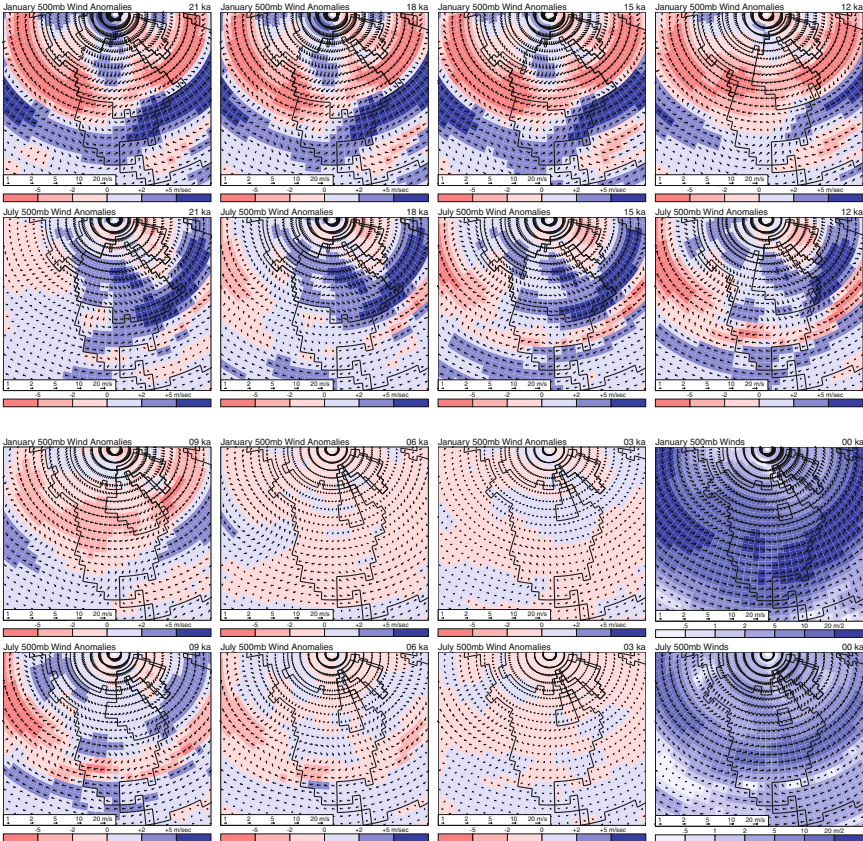


**Fig. 1.11** As in Fig. 1.8, except for upper-level (i.e. 500 mb) wind speeds (color) and present-day and anomalous components of 500 mb winds (arrows)

and is one of the robust features of paleoclimatic simulations over North America (Bartlein et al. 1998). Overall the wind-speed and direction anomalies, while spatially variable are quite similar over the interval from 21 to 12 ka, and the general pattern is still evident at 9 ka. Thereafter, there is little change in the upper-level circulation relative to the present day, with the small exception of a strengthened subtropical ridge over the southwestern U.S. from 12 to 6 ka.

The general trends in sea-level pressure between the LGM and present (Fig. 1.12) reflect the interplay of the “glacial-age” controls and the changing seasonal and latitudinal distribution of solar radiation, which during the summer, compete with one another in some ways during deglaciation. Between 21 and 15 ka, high pressure dominates over the ice sheet, while the Aleutian and Icelandic low-pressure systems are more strongly developed than present, particularly during winter. The surface-wind anomaly patterns clearly show the development of the “glacial anticyclone” with the anomalous flow-component spiraling outward

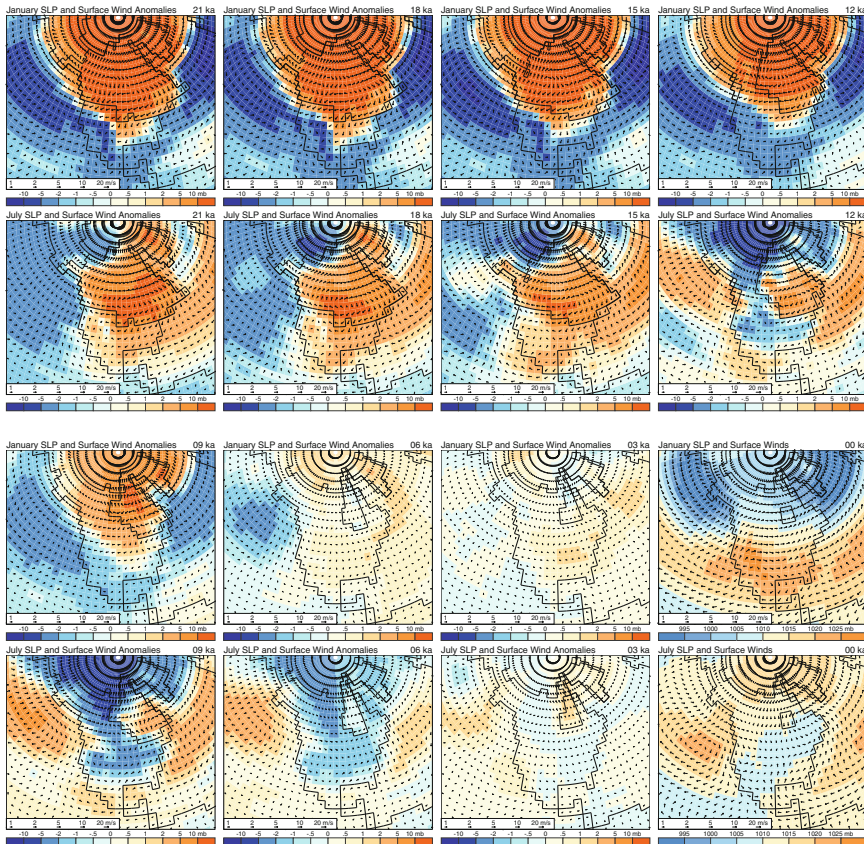


**Fig. 1.12** As in Fig. 1.8, except for sea-level pressure (color) and present-day and anomalous components of surface winds

in a clockwise direction from the center of the ice sheet, generating stronger-than-present northeasterly winds along the southern margin of the ice sheet, and stronger-than-present southerly and southeasterly winds along its western margin. (The distinction between the anomalous-flow components at a particular time is important, because the wind-flow anomalies could be read as “prevailing” or even “perpetual” winds, which they are not.) The influence of the ice sheet on surface winds remains evident even along the relatively small ice sheet at 9 ka. As the surface winds descend from the interior to the margins of the ice sheet they warm adiabatically, not sufficiently to be apparent in the large-scale temperature anomalies, but possibly enough to suppress precipitation (Webb et al. 1998).

By 12 ka, the summer insolation anomaly was sufficient to produce large positive anomalies in net radiation (Fig. 1.9) and near-surface air temperature (Fig. 1.10), except directly over the ice sheet, and this is reflected by low pressure over the continents from 12 to 6 ka. The pattern of mid-continental heating and the

development of lower-than-present pressure over the continents and attendant on-shore flow is another robust feature of paleoclimatic simulations of Northern Hemisphere summer climates during the insolation maximum (Kutzbach and Guetter 1986; Kutzbach et al. 1993; Harrison et al. 2003). The onshore-flow component of this package of responses to the insolation forcing is most evident over the combined landmasses of Europe, northern Africa and Asia where it leads to the enhanced early Holocene monsoon circulation in those regions, but it is also expressed in southern and southwestern North America (Thompson et al. 1993; Harrison et al. 2003; Alder and Hostetler in review), where the surface low pressure is accompanied by the development of a stronger-than-present subtropical ridge in summer from 12 to 6 ka (Mock and Brunelle-Daines 1999; Mock and Bartlein 1995; Harrison et al. 2003). After 6 ka, circulation patterns over North America approach those at present, with only very small anomalies noticeable at 3 ka.

#### ***1.4.5 Precipitation, Soil Moisture and Their Controls***

The availability of water for sustaining soil moisture levels and runoff, plant growth and lake levels, depends on net moisture which is the difference between precipitation inputs and evapotranspiration and evaporation outputs (P-E). Net moisture variations are recorded directly and indirectly in paleoecological, geochemical, hydrological and geomorphological records that, along with records that directly reflect temperature, provide the bulk of the record of terrestrial paleoclimates. There are two major controls of precipitation: (1) the availability of atmospheric moisture, and (2) the mechanisms for the release of that moisture that typically involve large-scale uplift and consequent adiabatic cooling and condensation. More than 90 % of the total moisture is contained by the atmosphere below the 500 mb level and approximately 50 % of the total moisture occurs below the 850 mb level (Pielke and Oort 1992). Atmospheric moisture thus can be indexed by the specific humidity at the 850 mb level (typically around 1500 m). Specific humidity is closely related to temperature though the Clausius-Clapeyron relation (saturation vapor pressure is a function of temperature), but can also be limited by low evaporation (Li et al. 2013). From the LGM to present, the GENMOM simulations of specific humidity at the 850 mb level (Fig. 1.13) indicate that the lower atmosphere was drier than present much of the time. In January over the interval from 21 to 12 ka, the only substantial positive anomalies of specific humidity are located over Beringia, corresponding to the region of positive temperature anomalies. In July, and particularly over the ice sheet, specific humidity anomalies again closely track temperature, except in the region of strong onshore flow in the southwestern part of the continent at 21 and 18 ka, and over the mid-continent from 12 to 6 ka, where soil-moisture anomalies are negative (Fig. 1.17), suggesting atmospheric moisture limitation through reduced evapotranspiration there.

The large-scale vertical motions (uplift or subsidence) in the atmosphere that enhance or suppress precipitation are described by vertical velocity ( $\omega$ ) at the

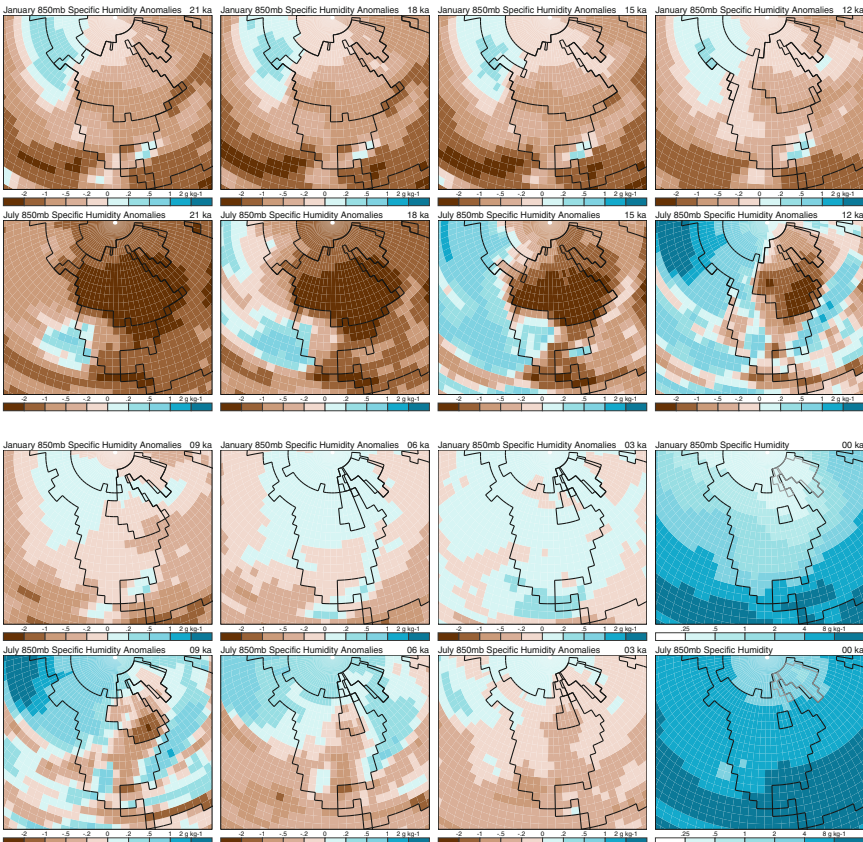


**Fig. 1.13** As in Fig. 1.8, except for specific humidity at the 850 mb level

500 mb level (Fig. 1.14) which is expressed using pressure as opposed to altitude as the vertical coordinate (in units of  $\text{Pa s}^{-1}$ ). Rising motions are of negative sign and subsiding motions are of positive sign because atmospheric pressure decreases with altitude. Rising motions in the atmosphere, and the consequent adiabatic cooling enhances the formation of clouds and precipitation under and downstream of upper-level troughs (negative 500 mb height anomalies), and in regions of steep horizontal temperature gradients (fronts). In contrast, subsiding motions and the associated adiabatic warming tend to suppress cloud formation and precipitation under upper-level ridges (positive 500 mb height anomalies). The interpretation of anomalies of omega is not as straightforward as is that for temperature or atmospheric specific humidity, because a negative anomaly could indicate stronger uplift or weaker subsidence (recall that omega is negative for rising motions), and the positive anomalies could indicate greater subsidence or weaker uplift.

In comparison with the anomalies of specific humidity (Fig. 1.13), the coherent anomaly patterns of omega (Fig. 1.14) are more limited spatially, reflecting the

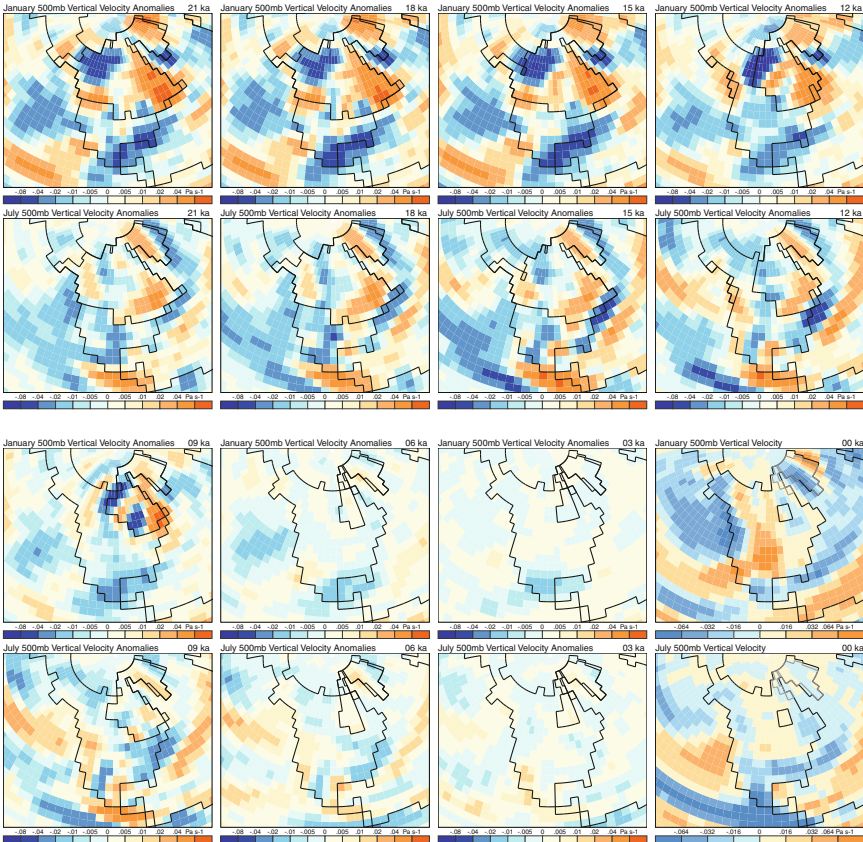


**Fig. 1.14** As in Fig. 1.8, except for 500 mb omega (vertical velocity). The simulated present-day values in January and July are shown in the last column of the bottom two rows, positive values (orange) indicate broad-scale subsidence, negative values (blue) indicate uplift. All other maps are (paleo) experiment minus (present-day) control anomalies, or differences in long-term means. Positive anomaly values (orange) indicate greater subsidence or less uplift than present, while negative values (blue) indicate greater uplift or less subsidence than present

greater range in scale of atmospheric circulation features that generate vertical motions. From 21 to 12 ka, a strong contrast in the omega anomalies exists around the LIS, with rising air on the northwestern quadrant of the ice sheet, and subsiding air along the eastern and southern margin. South of the ice sheet, during this interval a continent-wide region of rising motions prevails in both January and July which is associated with the region of higher-than-present winds caused by southward-displaced jet stream (Fig. 1.10). During the interval of high insolation in July (15 to 6 ka) a distinct region of increased uplift is associated with the enhanced North American monsoon (Mock and Brunelle-Daines 1999; see also Harrison et al. 2003 for discussion).

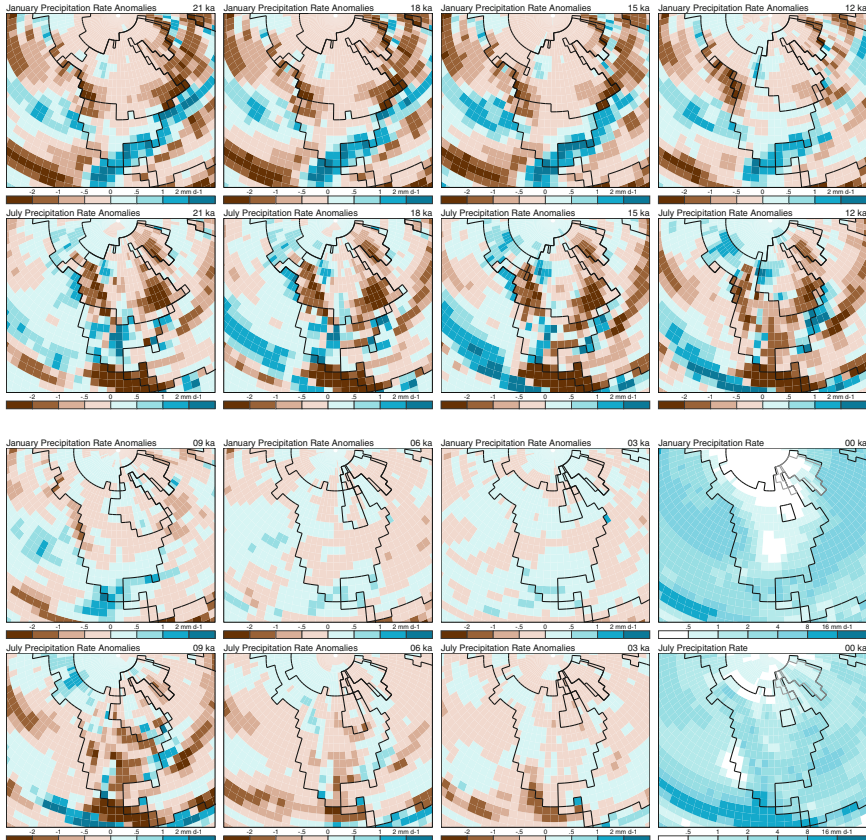


**Fig. 1.15** As in Fig. 1.8, except for precipitation

The anomaly patterns of precipitation (Fig. 1.15) follow those of omega closely overall, but exhibit some greater smaller-scale variability, as well as an overall tendency to be generally negative during glacial times. The resolution of GEN-MOM is about  $3.75^\circ$  latitude  $\times$   $3.75^\circ$  longitude which is relatively coarse and, while it would be tempting to explain this finer-scale variability in precipitation anomalies as consequence of equally fine-scale topography, the likely explanation lies in the specific controls of precipitation. In any case, it is difficult to find any substantial precipitation anomaly that is not also expressed by omega, leaving little room for the anomalies of specific humidity to play a limiting or enhancing role on the pattern of precipitation. Over the mid-continent in July from 12 to 6 ka, there is a tendency for the precipitation anomaly to be more negative than would be implied by the (positive, therefore greater subsidence) omega anomaly. As pointed out previously, this is also a region where negative soil moisture anomalies prevail.

To fully understand the anomaly patterns of soil moisture, which more directly influence the different kinds of paleoclimatic evidence that are used to reconstruct

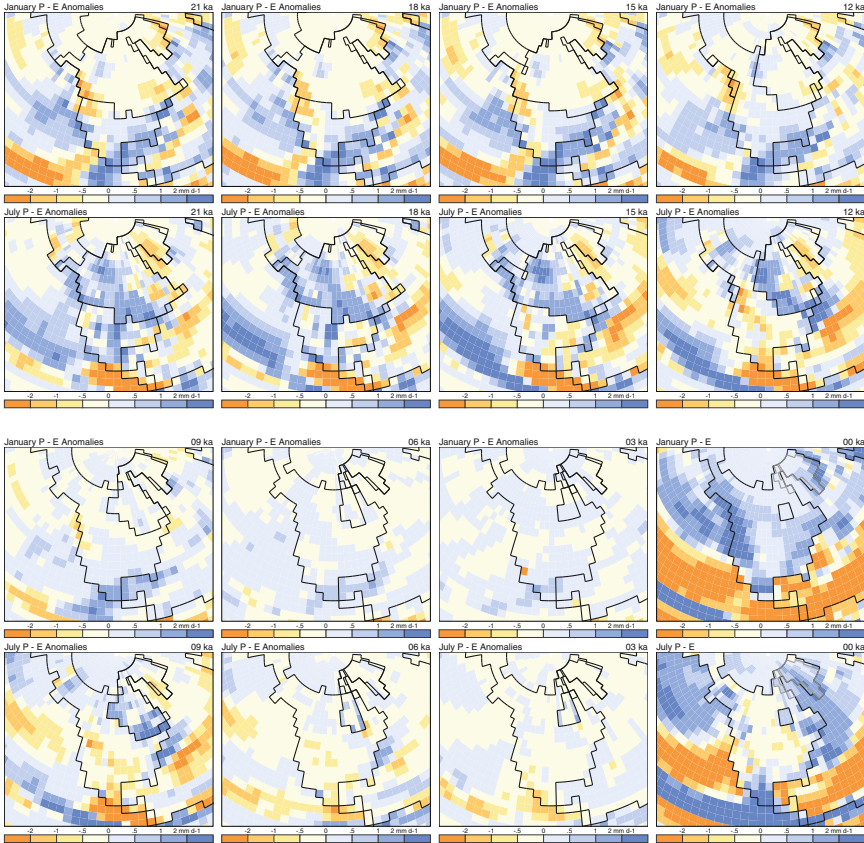


**Fig. 1.16** As in Fig. 1.8, except for P-E (precipitation minus evaporation). The simulated present-day values in January and July are shown in the last column of the bottom two rows, positive values (blue) indicate that long-term mean precipitation exceeds evaporation, negative values (orange) indicate evaporation exceeds precipitation. All other maps are (paleo) experiment minus (present-day) control anomalies, or differences in long-term means. Relative to present, positive anomaly values (blue) indicate greater precipitation or less evaporation or both and negative values (orange) indicate greater evaporation or less precipitation or both

past climates, it is first necessary to examine the anomaly patterns of P-E (Fig. 1.16). As previously discussed, evapotranspiration is controlled by both energy and moisture availability, which can be gauged here by the net radiation (Fig. 1.9) and precipitation anomalies (Fig. 1.15), and also by referring to omega (Fig. 1.14). Although net radiation anomalies are driven largely by insolation (and surface albedo, as over the ice sheets), the net-radiation anomalies also reflect to some extent the anomalies of omega. In particular, regions of large-scale subsidence, which tend to also feature negative anomalies of cloud cover (not shown), may display positive net-radiation anomalies because reduced cloud cover leads to positive incoming shortwave radiation anomalies that are greater than the negative

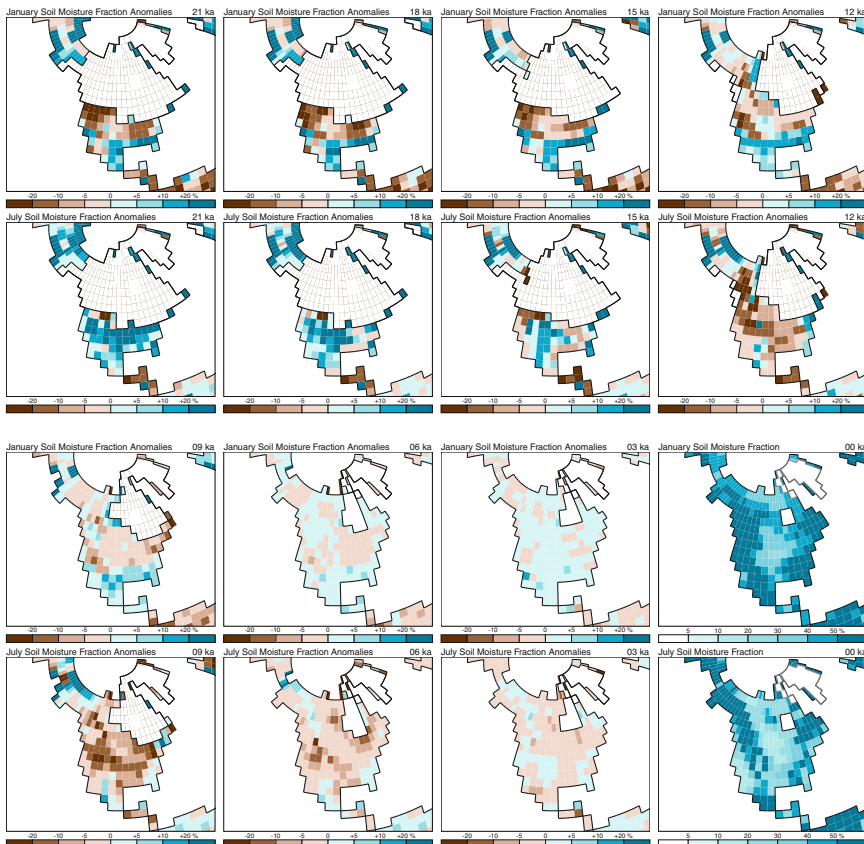


**Fig. 1.17** As in Fig. 1.8, except for soil-moisture fraction

anomalies of incoming long-wave radiation associated with less cloud radiative feedback. Examples of this effect can be seen in the eastern tropical Pacific in January from 21 to 15 ka, and over Central America in July from 21 to 9 ka (compare Figs. 1.9 and 1.14). As a consequence, except over the ice sheets where net radiation is strongly affected by albedo, owing to the dominant control of precipitation by omega, the anomaly patterns of P-E strongly resemble those of omega (Fig. 1.16). A major deviation from this pattern is evident over much of the conterminous U.S. in July during the interval from 12 to 6 ka, when the negative omega anomalies (i.e. increased uplift) in the southwest are surrounded by regions of positive anomalies (increased sinking, see Harrison et al. 2003, for further discussion). In contrast, July P-E anomalies tend to be uniformly (weakly) negative across this region and interval.

Soil moisture anomalies (Fig. 1.17) generally follow the trends in P-E (Fig. 1.16), with the exception of July anomalies in Beringia from 21 to 15 ka, where soil moisture anomalies are positive and P-E anomalies are mostly negative

or mixed. This pattern is explained by fact that soil moisture (as defined in the model output here) includes both free and frozen water. South of the LIS, January soil moisture anomalies are generally negative over the interval from 21 to 12 ka (particularly in the northwestern U.S.) and switch sign to positive anomalies along the southern edge of the continent, in the region of enhanced westerlies and precipitation. In July, soil moisture anomalies south of the ice sheet are positive from 21 through 15 ka, reflecting the generally lower-than-present evaporation rates then. After 9 ka, January soil moisture anomalies are relatively small, while July anomalies are generally negative, except for the small region of positive anomalies associated with the greater-than-present precipitation anomalies related to the stronger North American monsoon then (Harrison et al. 2003).

When the individual variables are examined jointly (Figs. 1.8, 1.9, 1.10, 1.11, 1.12, 1.13, 1.14, 1.15, 1.16, 1.17), the January anomalies are seen to change gradually from a “glacial mode” over the interval from 21 through 15 ka, to a transitional or “deglacial” mode represented by the 12 and 9 ka simulations, and then to a “Holocene” mode that shows a gradual relaxation of the anomalies to present. July anomalies display more variations than those for January, with elements of the transitional patterns appearing as early as 15 ka (e.g. warming in regions distant from the ice sheets). The transition culminates at 12 and 9 ka, when the July insolation maximum is reached, and this “early Holocene” regime then relaxes toward the present (with elements of its characteristic anomaly patterns still noticeable for many variables at 6 ka). These different responses are to first order a simple reflection of the magnitude of the insolation anomalies which are quantitatively larger for July than for January. The impact of the ice sheet as well as the lower GHGs during glacial times are registered in both January and July in the first part of the sequence, but remain influential longer in July than in January as the ice sheets retreat. We discuss the specific trajectories of seasonal climate from the LGM to present in more detail below.

#### ***1.4.6 Comparisons of the Simulations with Paleoclimatic Evidence***

Although networks of time series of paleoclimatic data exist for North America (e.g. pollen data, Williams et al. 2004), and quantitative reconstructions of past climates have been made for many individual records, syntheses of reconstructions are available only for the Holocene (Viau et al. 2006) or for the key periods of 21 and 6 ka (Bartlein et al. 2011). The latter synthesis provides reasonably good coverage at 6 ka, and enough coverage at 21 ka to resolve continental-scale patterns of temperature and precipitation (Fig. 1.18). The data shown in Fig. 1.18 are registered on a  $2^{\circ}$  latitude  $\times$   $2^{\circ}$  longitude grid, without interpolation, from the individual site reconstructions. (See Bartlein et al. (2011) for a discussion of the definitions of the two time slices and for the details of the synthesis.) Comparisons

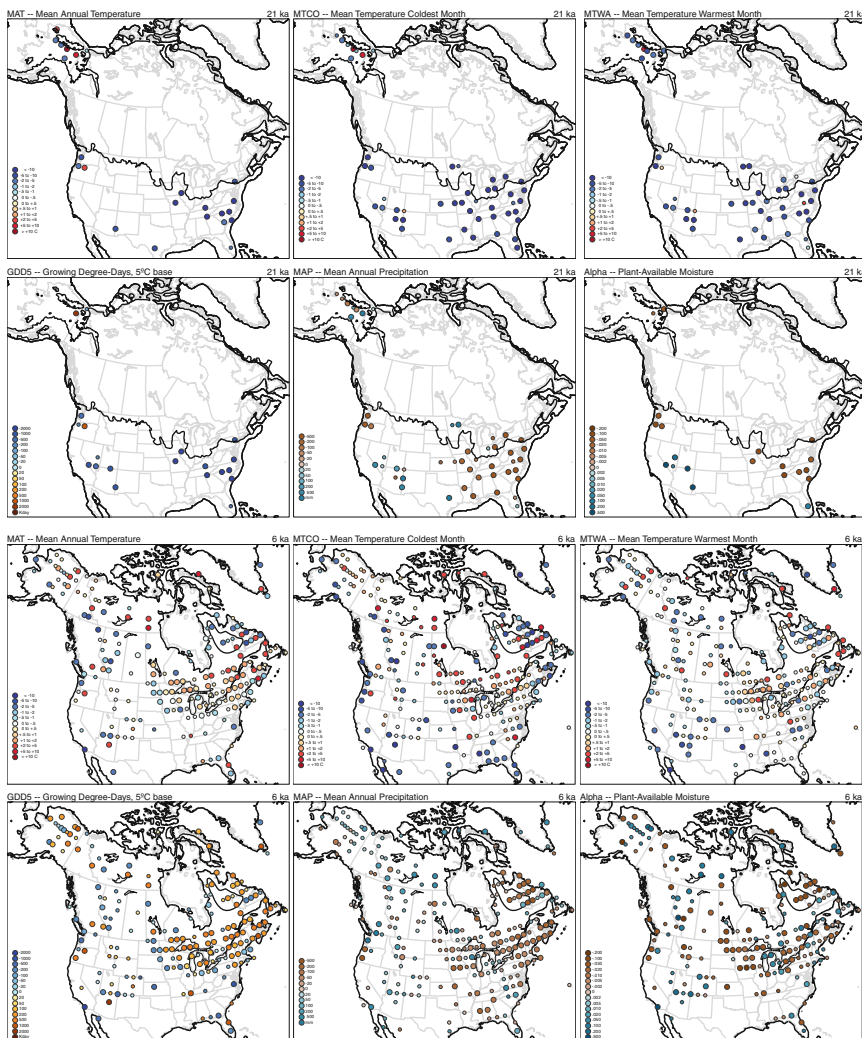


**Fig. 1.18** Pollen-derived reconstructions paleoclimatic data, 21 ka (LGM) and 6 ka (Mid-Holocene) (Bartlein et al. 2011). The data shown are anomalies (past minus present-day) of individual site reconstructions aggregated (without interpolation) onto a 2-degree grid

between the simulations and reconstructions must consider the different spatial resolution of the model and of the reconstructions, which are able to “sense” much finer-scale details of climate, such as those associated with topography that is necessarily smoothed at the resolution of GENMOM. (See Bartlein and Hostetler (2004) and Harrison and Bartlein (2012) for a discussion of the consequences of model resolution in comparing simulations and observations.) At 21 ka, the temperature reconstructions (mean annual temperature (MAT)), the mean temperature

of the coldest month (MTCO), the mean temperature of the warmest month (MTWA) and growing degree-days, with a 5 °C base (GDD5) all display the expected generally lower-than-present values. In Beringia, however, the reconstructions are mixed, and some provide support for the warmer-than-present conditions apparent in the simulations. Mean annual precipitation (MAP) and plant-available moisture (alpha, the ratio of actual equilibrium evapotranspiration to potential evapotranspiration) both show the latitudinal pattern of moisture anomalies in the simulations, with generally drier-than-present conditions south of the ice sheet, and wetter-than-present conditions at lower latitudes.

The reconstructions for MTWA and GDD5 at 6 ka show the higher-than-present temperature anomalies apparent in the simulations, with a hint of lower-than-present temperatures around Hudson Bay, which covered a larger area then than at present due to isostatic depression by the LIS. Reconstructed summer temperatures were cooler than present in the southwestern U.S., which is at odds with the simulations. Reconstructed MAP and alpha show a consistent pattern of drier-than-present conditions in the Pacific Northwest, wetter-than-present conditions in the Southwest, and drier-than-present over the mid-continent and eastern North America. Both the simulations and reconstructions provide support for enhancement of the North American monsoon in the mid-Holocene as a consequence of greater-than-present summer insolation, as elsewhere around the world (Liu et al. 2004), and for mid-continental aridity. Overall, there do not seem to be any major discrepancies between the reconstructions and simulations that would discount the use of the simulations and reconstructions jointly for understanding the nature and controls of the broad-scale changes in climate between 21 ka and present.

#### ***1.4.7 The Trajectory of Seasonal Climate Changes***

Examination of the sequence of climate changes from the Last Glacial Maximum to present using only January and July is somewhat oversimplified owing to the diversity of the insolation anomaly time series for other months of the year (e.g. for 45 °N, Fig. 1.19). Each month's time series is a unique sinusoid and the phase (evidenced by the time of the maximum insolation anomaly in each month over the interval 22 ka to present) varies. The maximum anomaly occurs in January around 22 ka, in April around 14 ka, in July around 10 ka and in October around 4 ka. The specific insolation curves also vary latitudinally (see Fig. 1.4 in Harrison and Bartlein (2012) for illustration). The likely consequences of these variations in insolation are corresponding variations in temperature, mediated by atmospheric circulation patterns and surface water- and energy-balances. Such variations in temperature can be examined with the transient climate simulations conducted with CCM3 by Liu et al. (2009) which have been summarized by season over the interval 22 ka to present. These transient simulations were “forced” with a set of boundary conditions or controls similar to those used for GENMOM (e.g. Fig. 1.7), with additional prescribed forcing of fresh-water inputs to the oceans to

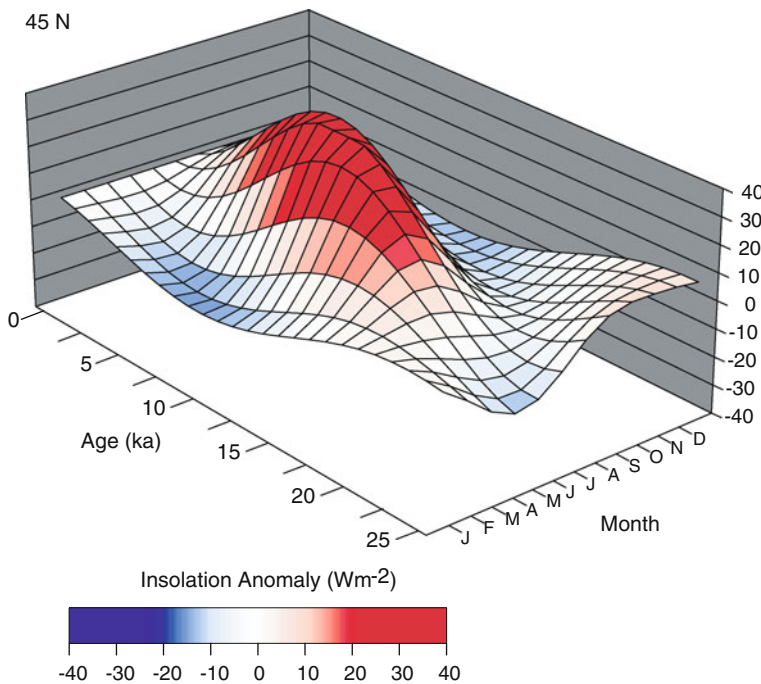


**Fig. 1.19** Variations in monthly insolation at 45°N, 25 ka to present

trigger abrupt changes in the AMOC (Fig. 1.5) as they do in the real climate system.

The decadal time-step temperature simulations for the year (Ann) and individual seasons (winter, December–March (DJF); spring, March–May (MAM); summer, June–August (JJA); and autumn, September–November (SON)) are shown in Fig. 1.20 for selected grid cells (to avoid spatial smoothing) around North America for 22 ka to present (left-hand panels in each set) and 11 ka to present (right-hand panels). Locations (grid cells) distant from the ice sheet and the North Atlantic (i.e. the Southwest (Fig. 1.20e), Southeast (Fig. 1.20f) and Pacific Northwest (Fig. 1.20d) display the smoothest curves overall, while the temperature curves for the location adjacent to the North Atlantic (“Northeast,” Fig. 1.20c) and in Beringia (Fig. 1.20a) display abrupt changes, particularly during deglaciation. The more abrupt changes include the rapid warming at the beginning of the Bølling–Allerød chronozone (14.7 ka), variability within the chronozone, including several sharp cooling trends, particularly those at the beginnings of the Inter-Allerød cold period (13.2 ka), and the Younger Dryas chronozone (12.9 ka), and the abrupt warming at the end of the Younger Dryas chronozone (11.7 ka). The last abrupt change related to an imposed change in fresh-water input to the North Atlantic occurs at 8.2 ka, and is clearly seen in the simulated temperatures for the Northeast location.

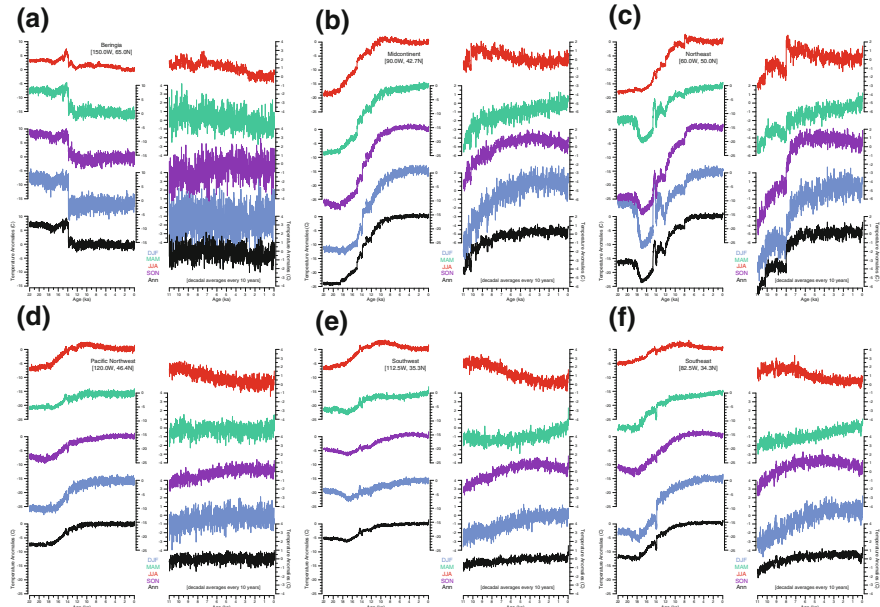


**Fig. 1.20** Regional variations in transient simulations (Liu et al. 2009) of 2 m air temperature for individual grid cells representing specific locations from 22 ka to present (left-hand panels) and 11 ka to present (right-hand panels). **a** Beringia, **b** Midcontinent, **c** Northeast, **d** Pacific Northwest, **e** Southwest, **f** Southeast. From top to bottom in each stack, the curves are for summer (JJA), spring (MAM), autumn (SON) and winter (DJF), and annual values. The values shown are seasonal (or annual) averages, plotted every ten years. Scales differ among regions, but have the same ranges for the 22–0 ka and 11–0 ka curves

In Beringia, a somewhat counter-intuitive abrupt cooling in all seasons occurs around 13.5 ka (when the rest of the continent was warming) when the LIS specified as a boundary condition became too small to induce the southerly flow that sustained warmer-than-present conditions that persisted during early periods of the simulations. Overall, the seasonal temperature simulations from 22 ka to present reflect the combination of several components: (1) global climatic change from the LGM to present, (2) changes in the latitudinal and seasonal distribution of insolation, and (3) region-specific changes attributable to modified atmospheric circulation related to the size of the ice sheets.

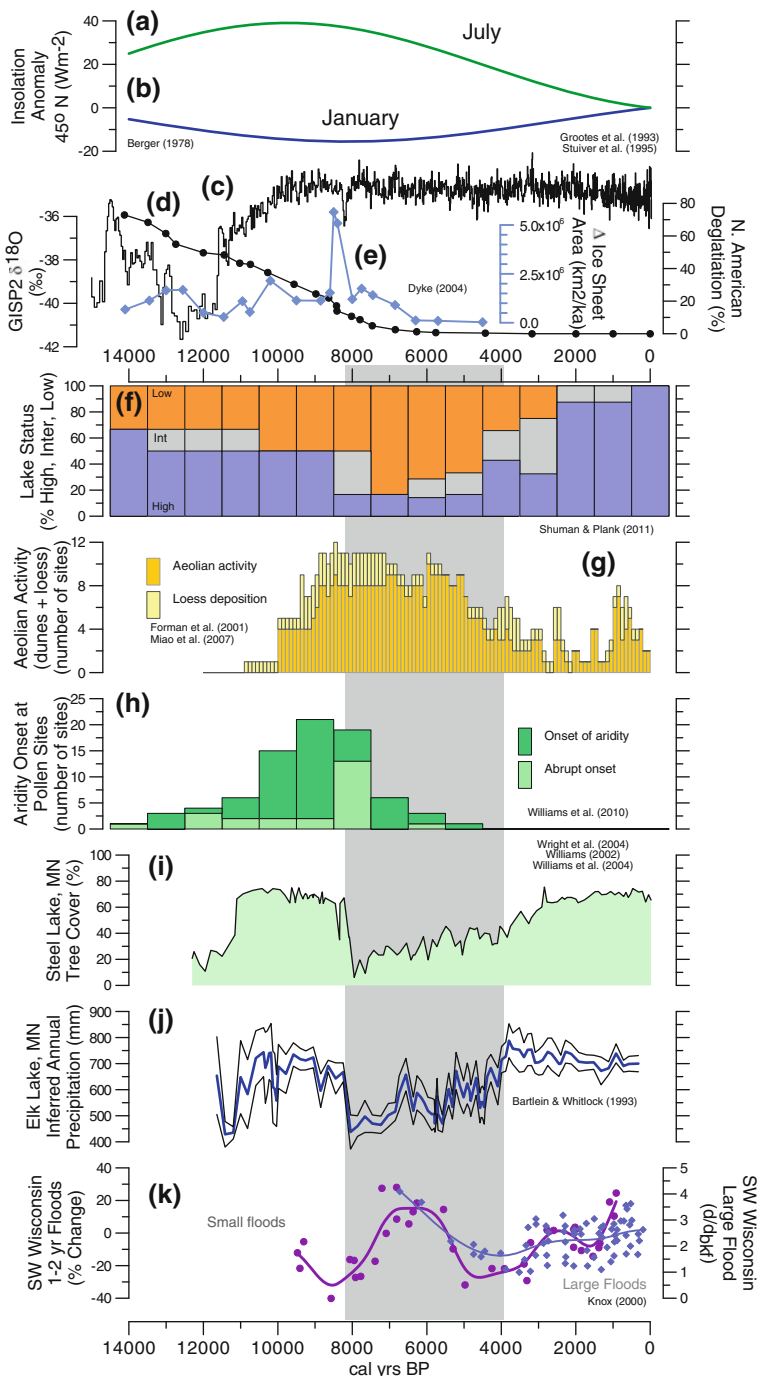
During the Holocene (right-hand panels in Fig. 1.20), regional variations in the temperature trends during different seasons become evident. The simulated temperatures for the Southwest location (Fig. 1.20e) show what might be regarded as the canonical Northern Hemisphere temperature history, with summer (JJA) temperatures reaching a maximum in the early Holocene and decreasing thereafter and with winter (DJF) temperatures increasing steadily throughout the Holocene, in opposition to the summer trend. Spring (MAM) temperatures increase in the late Holocene, while autumn (SON) temperatures decrease. Summer temperatures in

the different regions are generally similar, showing a decrease over the Holocene (except before 8.2 ka in the Northeast (Fig. 1.20c), when the impact of deglaciation and ocean–atmosphere interactions were still dominating). The coherence of the summer temperature trends among regions is likely related to the strong summer insolation forcing. Autumn (SON) and winter (DJF) temperatures show similar trends over the Holocene, but vary more than summer temperatures do among regions, with little trend (but considerable variability) in Beringia and the Pacific Northwest (Fig. 1.20a, d), and a tendency for slight cooling in the late Holocene in the midcontinent (Fig. 1.20b). The trends in spring (MAM) temperatures vary considerably among regions, decreasing over the Holocene in Beringia (Fig. 1.20a), showing little trend in the Pacific Northwest (Fig. 1.20d), increasing faster in the early Holocene and more slowly in the late Holocene in the mid-continent and Northeast locations (Fig. 1.20b, c), decreasing in the early Holocene and increasing in the late Holocene in the Southwest location (Fig. 1.20e), and increasing almost linearly in the Southeast (Fig. 1.20f).

The variety of seasonal trends in the different regions (in these CCM3 simulations) considerably broadens the range of potential climate changes that could be invoked to explain the records of various paleoclimatic indicators. In the past, recognition of the independence of the trends in different seasons has allowed reconciliation of apparently contradictory records (Harrison et al. 1993; Bonfils et al. 2004). However, just as quite complicated mathematical functions or time series can be well approximated by Fourier series, the availability of a variety of seasonal trends could lead to explanations of the trend in paleoenvironmental indicators that fit the paleo data well, but lack any real mechanistic support.

## 1.5 The Holocene

During the Holocene (the past 11.7 kyr), the specific details of paleoclimatic sequences have varied among regions (Viau et al. 2006, see their Fig. 1.3; also Shuman 2012), which are all part of the general trend of climate toward the present day following the demise of the LIS and the gradual approach of insolation and atmospheric composition toward their present values. Superimposed on these individual trends is the widespread phase of aridity in the interior of North America between 8 and 4 ka (with some regional variation in its specific timing; Harrison et al. 2003; Cook et al. 2008). A variety of paleoenvironmental indicators reflect the spatial extent and timing of this “Mid-Holocene Drought” (Fig. 1.21), and in general suggest that dry conditions increased in intensity during the interval from 11 to 8 ka, became widespread between 8 and 4 ka, and then gave way to increased moisture after 4 ka. Lake-status indicators at 6 ka indicate lower-than-present levels (and hence drier-than-present conditions) across much of the continent (Shuman and Plank 2011), and quantitative interpretation of the pollen data in (Williams et al. 2004) suggests a similar pattern of aridity, but again with some regional and local variability, such as moister-than-present conditions in the



◀ **Fig. 1.21** Synthesis of records from the mid-continent, showing the onset of aridity during the mid-Holocene. Figure redrawn and updated from (Cook et al. 2008). **a** July insolation (anomalies) at 45°N; **b** January insolation (anomalies) at 45°N (Berger 1978); **c** GISP2  $\delta^{18}\text{O}$  (Grootes et al. 1993; Stuiver et al. 1995); **d** progress of North American deglaciation (Dyke 2004); **e** change in ice-sheet area (Dyke 2004); **f** lake status (Shuman and Plank 2011); **g** aeolian activity (Forman et al. 2001; Miao et al. 2007); **h** pollen indicators of aridity onset (Williams et al. 2010); **i** tree cover at Steel L. Minnesota (Williams et al. 2004; Williams 2002; Wright et al. 2004); **j** inferred precipitation anomalies from pollen for Elk L. Minnesota (Bartlein and Whitlock 1993); **k** flood-magnitude variations from southwestern Wisconsin (Knox 2000)

Southwestern United States (Williams et al. 2010; Williams et al. 2009; Thompson et al. 1993). Although the region of drier-than-present conditions extends into the Northeastern United States and eastern Canada, most of the paleoclimatic evidence for mid-Holocene drought is focused on the midcontinent, in particular the Great Plains and Midwest, where the evidence for aridity is particularly clear. There, the expression of middle Holocene dry conditions in paleoenvironmental records has long been known, as for example the “Prairie Period” evident in fossil-pollen data (see Webb et al. 1983), and the recognition of significant aeolian activity (dune formation) on the Great Plains (Forman et al. 2001; Harrison et al. 2003) that would be further favored by a decrease in stabilizing vegetation cover.

Temporal variations in the large-scale controls of North American regional climates and some of the paleoenvironmental indicators of the moisture changes are shown in Fig. 1.21. In addition to insolation forcing (Fig. 1.21a, b), the size of the LIS was a major control of regional climates, and while diminished in size from its full extent at the LGM (21 ka), the residual ice sheets at 12 and 9 ka (Fig. 1.20d, e) still influenced atmospheric circulation over eastern and central North America in climate simulations for those later times.

The records of aridity indicators for the midcontinent generally show relatively dry conditions between 8 and 4 ka. Lake-status records (Fig. 1.21f, Shuman and Plank 2011) show the highest frequency of lakes at relatively low levels during the interval between 8 and 4 ka, and a higher frequency of lakes at relatively high levels before and after that interval. Records of widespread and persistent aeolian activity and loess deposition (dust transport) increase in frequency from 10 to 8 ka, and then gradually fall to lower frequency in the late Holocene, with a noticeable decline between 5 and 4 ka. Pollen records of the vegetation changes that reflect dry conditions (Fig. 1.21g; Williams et al. 2010; Williams et al. 2009) show a somewhat earlier onset of dryness than do the aeolian or lake indicators, reaching maximum frequency around 9 ka. Increased aeolian activity also occurred during the last 2000 years (Fig. 1.21f; Forman et al. 2001; Miao et al. 2007), but was less pronounced than during the mid-Holocene.

The pollen record from Steel Lake, MN (Wright et al. 2004), expressed in terms of tree-cover percentages (see Williams 2002, for methods) provides an example to illustrate a pattern of moisture-related vegetation change that is typical of many sites in the Midwest, with an abrupt decline in tree cover at this site around 8 ka, over an interval equal to or less than the sampling resolution of the record (about 200 years).

The decrease in tree cover and inferred moisture levels is followed by relatively low, but slightly increasing, inferred moisture levels for about 4000 years, with higher moisture levels after 4 ka. The magnitude of this moisture anomaly can be statistically inferred from the fossil-pollen data using modern relationships between pollen abundance and climate, as was done for the pollen record at Elk Lake, MN, which is near Steel Lake (Fig. 1.21j; Bartlein and Whitlock 1993; see also Webb et al. 1998). Expressed in terms of precipitation, the moisture decrease in the midcontinent needed to support these vegetation changes is about 350 millimeters per year ( $\text{mm y}^{-1}$ ), or about 1 millimeter per day ( $\text{mm d}^{-1}$ ), which are levels between 50 and 80 % of the present-day values.

The GENMOM simulations produce general large-scale subsidence and hence dry conditions in the interior of North America during the growing season (and an enhancement of the North American monsoon; see Figs. 1.14, 1.15, 1.16, 1.17). Like other GCM simulations, the GENMOM simulations are not quite as dry as can be inferred from the paleoclimatic data, with anomalies smaller than  $1 \text{ mm d}^{-1}$ . In contrast, precipitation and soil moisture simulations from a regional climate model (RCM; Diffenbaugh et al. 2006) are more comparable in magnitude to those recorded by the paleoenvironmental data, and suggest that some of the “undersimulation” of drying by GCMs is related to the resolution of the models. In general, simulations from both GCMs and RCMs are consistent with the paleoclimatic evidence, and reinforce our conceptual model of the controls of drought in the midcontinent (Shinker et al. 2006; Harrison et al. 2003). Although further diagnosis of simulated climates is warranted, the ultimate control of the aridity is likely the direct (through its impact on the surface energy and water balance) and indirect (through the generation of large-scale uplift over southwestern North America and subsidence in adjacent regions) effects of the summer insolation anomaly (Fig. 1.19).

The midcontinental drought during the middle Holocene thus provides an illustration of a significant hydrologic anomaly with relatively abrupt onset and ending that occurred in response to gradual changes in the main driver of Holocene climate change (insolation), reinforced by regional- and continental-scale changes in atmospheric circulation related directly to deglaciation and surface feedbacks. There are other examples of abrupt hydrological responses to gradual or large-scale climatic changes during the Holocene. For example, the development of wetlands and peatlands in the Northern Hemisphere began relatively early during the course of deglaciation but accelerated during the interval of high summer insolation between 12 and 8 ka (Charman et al. 2013; Gajewski et al. 2001; Yu 2012). Also, the frequency and magnitude of floods across a range of different watershed sizes also tracks climate variations during the Holocene (Fig. 1.21j; Knox 2000, 1993; Ely 1997), albeit in a complicated fashion, owing to dependence of flooding on long-term climate and land-cover conditions as well as on short-term meteorological events.

A second continental-scale trend in Holocene climate is long-term cooling in the Arctic, driven by summer insolation (Kaufman et al. 2004; Kaufman et al. 2009). The timing of the Holocene temperature maximum was time-transgressive,

starting earlier in Beringia and northwestern North America, and later in north-eastern North America, with the delay there related to the residual LIS (Fig. 1.6), and the general longitudinal asymmetry of atmospheric circulation and temperature in the Arctic. This long-term cooling is also apparent in Greenland ice-core records (Fig. 1.2d), and in a variety of paleoenvironmental indicators that span the past several thousand years (Kaufman et al. 2009). There is a tendency to regard the high-latitude summer temperature record as a general record of Northern Hemisphere temperatures; however, as the transient simulations in Fig. 1.20 suggest, the high-latitude summer temperature trends are really not generalizable to other seasons and latitudes.

On time scales shorter than the slow (relative to the time span) variations in insolation during the Holocene, there is abundant evidence of multidecadal-to-century time scale variations of climate (Cook et al. 2008; see section 4.4). There are several candidate explanations for these variations, including the continuing influence of the insolation changes, the impact of variations in solar output, volcanism, land-surface changes and “unforced” internal variations of climate, which will also be described below. One potential control of century-to-millennial time scale variations that has not been excluded as their cause is variation of solar output on similar time scales, and correlations between solar irradiance indicators and North Atlantic climate variability (Bond et al. 1997) and variations in terrestrial records (Gavin et al. 2011; Shuman and Plank 2011; Asmerom et al. 2007; Hu et al. 2003) have been established. However, there is no single index of solar irradiance variability during the Holocene, and the correlations are often computed only after considerable smoothing of the time series (which increases the likelihood of obtaining spurious correlations), and so such correlations should be regarded as interesting but not yet definitive (Committee on the Effects of Solar Variability on Earth’s Climate 2012).

The Holocene record shows that even with boundary conditions or large-scale controls of climate close to those of the present, large-scale, coherent variations of climate can occur, sometimes abruptly (Shuman 2012). Overall, however, the principal modes of climate variability, both global and regionally, continue to be driven by the gradual changes in boundary conditions, particularly insolation (Marcott et al. 2013).

## 1.6 The Last Millennium

The past thousand years or so provides another “natural” (albeit heavily human-influenced) experiment that can be examined with a combination of climate-model simulations and paleoclimatic data syntheses, and is therefore another focus for data-model comparisons (Braconnot et al. 2012). The advantage of this interval stems from a relatively well understood controls of climatic variations (Schmidt et al. 2011), and the availability of paleoenvironmental data with annual resolution (PAGES 2k Consortium 2013; Mann et al. 2008). The general variations in climate

over this interval can be characterized as those that primarily result from the natural variability in the controls of climate (and from internal variability) prior to 1700 or 1750 CE, and those that result from strong anthropogenic forcing of climate afterward, that lead to the prominent “hockey stick” (Committee on Surface Temperature Reconstructions for the Last 2000 Years 2006) appearance of many records of climate or other environmental systems (Steffen et al. 2011; Cornell et al. 2012).

### 1.6.1 Controls of Climate Over the Past Millennium

The utility of the last millennium as a focus for climate-modeling experiments has motivated the assembly of the boundary conditions required to produce simulations of climate that can “track” observed climate on a year-to-year basis (Schmidt et al. 2011). Such “forced-variability” simulations contrast with the other paleo-experiments discussed above, where only the long-term mean values of the boundary conditions are specified, and so the simulations can show only “unforced (or “free”) variability” from one year of the simulation to the next. (Simulation of the last millennium is currently underway using a variety of different climate models, and the simulations are now being examined in detail, e.g. Bothe et al. 2013; Landrum et al. 2013.) The main controls of climate that varied over the past millennium appear in Fig. 1.22 (left), and can be compared with one another by expressing each in terms of its radiative forcing potential, i.e. as a perturbation of the long-term mean Earth-Atmosphere energy balance (Forster et al. 2007). (Note that the scales differ from curve to curve in Fig. 1.22.)

“Well mixed” GHGs ( $\text{CO}_2$ ,  $\text{CH}_4$ , etc.), exhibit the classic “hockey stick” pattern, varying little from their preindustrial values until around 1750 CE, when they began to increase exponentially, contributing  $+2.5 \text{ Wm}^{-2}$  to the global energy balance over this period (relative to earlier) (Fig. 1.22). Solar irradiance variability is shown as four curves to graphically illustrate the uncertainty that exists in the specification of its record, but the amplitude of the radiation variations are only about one-tenth of those of the GHGs. The curve labeled “LULC” represents the impact on the energy balance of the increases in albedo that accompany the conversion of natural vegetation to agriculture, and has a negative impact on the energy balance of roughly the same magnitude as that of solar forcing but opposite in sign over the past 250 yrs. Reductions in atmospheric transparency from volcanic eruptions force the largest amplitude of perturbations in radiative forcing, but the perturbations are short in duration, lasting only a year or so following large eruptions. Not shown on Fig. 1.22 are the orbitally driven changes in insolation (e.g. Figs. 1.19 and 1.21), which include decreases of around  $4 \text{ Wm}^{-2}$  in late summer and increases of around  $3 \text{ Wm}^{-2}$  in spring at mid- and high latitudes in the Northern Hemisphere. The important trend in the controls of climate is therefore that of the GHGs, and its exponential increase after 1750 CE, with volcanism having large, but short-term impacts on top of that trend.

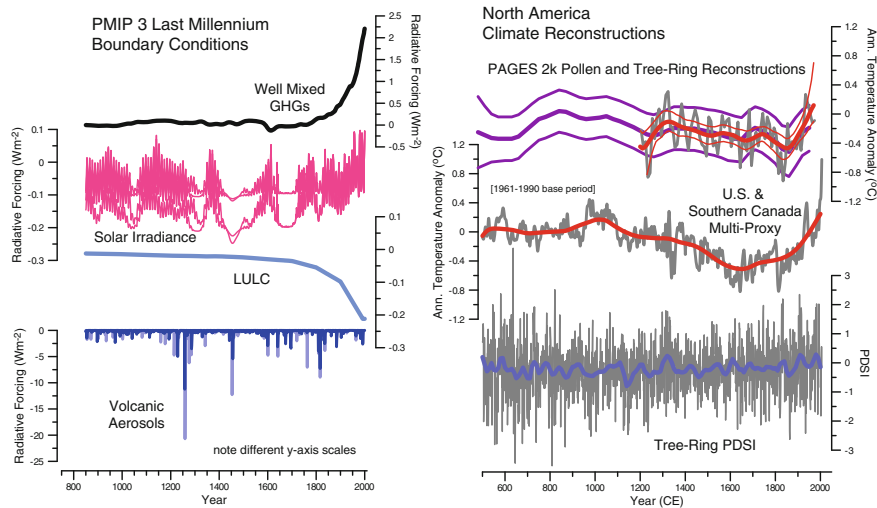


**Fig. 1.22** Boundary conditions (large-scale controls of climate) for the last millennium (*left*). (Schmidt et al. 2011). (*top*) well-mixed greenhouse gases, mainly carbon dioxide; solar irradiance (four curves are shown reflecting uncertainty that underlies this control of climate); land-use land-cover change expressed in radiative-forcing terms for comparability with the other series; (*bottom*) impact on radiative forcing of volcanic aerosols. Climate reconstructions for North America (*right*). (*top*) (PAGES 2k Consortium 2013) tree-ring and pollen-derived temperatures, area-average (for the U.S. and southern Canada); reconstructions of annual temperature using multiple data sources (Mann et al. 2009); (*bottom*) tree-ring derived Palmer Drought Index (PDSI) values (Cook et al. 2004)

“Natural” or “free” variability of the climate system—the variability of climate that arises even in the absence of changes in external forcing—also becomes a consideration on the time-scales of variability that are evident over the past millennium. Such variations (also called “internal variations”) are common features of long climate simulations, and could rival in magnitude those variations that appear in simulations of the past millennium (Jungclaus et al. 2010). While such variations have occurred throughout Earth history, the focus now is separating these natural variations from anthropogenic ones, i.e., the task of “attribution and detection” studies (Hegerl et al. 2007). This topic is discussed in detail in the last chapter of this book.

### 1.6.2 Climate Reconstructions for North America Over the Past Millennium

Continental-scale reconstructions of temperature have been made using various kinds of paleoclimatic evidence, including pollen (Viau et al. 2006; PAGES 2k Consortium 2013), tree-rings (PAGES 2k Consortium 2013), and networks of multiple kinds of paleoclimatic evidence (so-called “multiproxy” data sources;

Mann et al. 2009; Mann et al. 2008). The reconstructed temperatures (Fig. 1.22, right) generally track the orbitally driven decrease in summer insolation over time and increase in GHGs after 1750, with a cool episode between 1600 and 1800 CE, known generally as the Little Ice Age (LIA), preceded by a generally warmer interval prior to 1200 CE, often referred to as the Medieval Climate Anomaly (MCA). The recent “PAGES 2k” synthesis (PAGES 2k Consortium 2013) suggests that while similar warm and cold intervals exist in other regions they are not strictly synchronous globally. Moisture variations, expressed as Palmer Drought Severity Index (PDSI) values (Cook et al. 2004); Fig. 1.22, negative values indicate drier conditions), have also been reconstructed from tree-ring networks and show a tendency for episodic, multi-decadal droughts and wet intervals more so than long-term trends. These multidecadal dry intervals, have been referred to as “megadroughts” (Cook et al. 2004), and relative to droughts observed during the instrumental period (the past 150 yrs), are greater in magnitude and duration. Relative to Holocene droughts (Fig. 1.21), however, they are smaller, being registered by changes in the growth rate of living trees, as opposed to widespread tree mortality and replacement of forest by steppe.

## 1.7 Key Findings

The focus of this chapter has been on the paleoclimate of North America, on time spans that range from the Cenozoic to the last millennium. The main feature of that climate history is the great variability that occurs on all time scales. Except on the shortest of climatological time scales (interannual-to-decadal) the variations are largely explainable by the external controls of climate (on a specific time scale) and by internal feedbacks.

- Overarching findings:
  - Climate varies on all time scales, with longer-term variations generally larger in magnitude than shorter-term ones. There seems to be no particular warm or cold state of the climate system nor time when variability is not important.
  - Climate variations over the past few million years are both progressive and recurrent. Over this interval, the long-term mean state of climate shows both gradual cooling and a general increase in the amplitude of variation, with occasional abrupt changes in variability, such as the increasing importance of 100 kyr variation over the past million years. Superimposed on these general trends are repeated and rapid (on this long time scale) glacial/interglacial variations, and while recurrent and broadly similar to one another, the “cycles” differ in detail.
  - The principal driver of the recurrent climate variations is the variation in insolation related to changes in Earth’s orbit, which are amplified sufficiently to generate glacial-interglacial cycles.

- On shorter time scales, i.e. over the past 100 kyr, recurrent transitions between warm and cold mean states are also the prominent mode of variability of climate, and again, while broadly similar, each fluctuation differs in duration and character.
  - The higher-frequency variations of climate that are apparent in shorter records (e.g. for the last millennium) must also be present over longer spans of time, but the nature and resolution of longer records generally precludes their registration.
  - Higher-frequency variations are contingent on the long-term changes in the climate system that are expressed in longer term, and lower frequency records (e.g. the size of the ice sheets, atmospheric composition, or latitudinal and seasonal distribution of insolation).
- The last 21 kyr, from the Last Glacial Maximum to present, includes the full range of variations in the large-scale controls of climate and states of the climate system that have been experienced over the past million years and longer, and the scope of these variations thus provides a set of “natural experiments” that can be exploited through the comparison of climate-model simulations and paleoclimatic data syntheses.
  - The hierarchy of controls of the climate of individual locations or regions are clearly illustrated by the GENMOM simulations, and include
    - global and continental controls of climate (including the seasonal and latitudinal distribution of insolation, ice sheets and atmospheric composition), which govern the overall state of the climate and broad-scale net radiation and temperature patterns, including land/ocean and high-latitude/low-latitude contrasts;
    - the impact of the broad-scale temperature gradients and the North American ice sheets (when present) on upper-level and surface atmospheric circulation;
    - the general control by temperature of atmospheric moisture content;
    - the impact of atmospheric circulation on large-scale vertical motions (uplift and subsidence) moisture flux, and in turn, on precipitation;
    - the impact of the surface energy- and water-balances on evapotranspiration and soil moisture.
  - The general trends of North American climate change over the past 21 kyr differ among seasons.
    - Winter (January) conditions change gradually from a “glacial mode” over the interval from 21 through 15 ka, to a transitional or “deglacial” mode represented by the 12 and 9 ka simulations, and then to a “Holocene” mode that shows a gradual relaxation of the anomalies to present.
    - Summer (July) conditions show more variation, with elements of the transitional patterns appearing already at 15 ka (e.g. warming in regions distant from the ice sheets). The transition culminates at 12 and 9 ka, when the July insolation maximum is reached, and then this “early Holocene” regime also

relaxes toward the present (with elements of its characteristic anomaly patterns still noticeable for many variables at 6 ka).

- The different seasonal responses reflect the magnitude of the insolation anomalies which are quantitatively larger for July than for January. The impact of the ice sheets (as well as the lower GHGs during glacial times) are registered in both January and July in the first part of the sequence, but remain influential longer in July than in January as the ice sheets retreat, and atmospheric composition approaches its “pre-industrial” state.
- There is considerable regional variability in the trends of temperature in all of the seasons, reflecting the variations over time in the annual cycle of insolation. This variability can provide the basis for more elaborate explanations of the trends observed in paleoclimatic records, but also raises the prospect of describing spurious correlations.
- Continental-scale climate anomalies largely related to insolation forcing are also a principal feature of Holocene climates; these include:
  - the development of widespread aridity in the midcontinent, likely related to the direct (through the surface energy and water balances), and indirect (through atmospheric circulation) response to the positive summer insolation anomaly;
  - a concomitant amplification of the North American monsoon;
  - pervasive summertime cooling at high latitudes across North America.
- Over the past millennium, multidecadal and centennial-scale climate variations have occurred, some in response to variations in insolation, atmospheric composition (GHGs and aerosols), and changes in land-use/land-cover, and likely some in response to free or unforced variations. In the case of drought, these variations over the past millennium are larger than those described by the instrumental record, but small relative to those during the Holocene (the past 11,700 years).

**Acknowledgments** Research was supported by the U.S. National Science Foundation and the U.S. Geological Survey. We thank Zhengyu Liu and Bette Otto-Bliesner et al. for access to the TRACE21 transient climate-model experiment data. TRACE21 is supported by P2C2 program/NSF, Abrupt Change Program/DOE, EaSM program/DOE, INCITE computing program/DOE and NCAR.

## References

- Abe-Ouchi A, Saito F, Kawamura K, Raymo ME, Okuno Ji, Takahashi K, Blatter H (2013) Insolation-driven 100,000-year glacial cycles and hysteresis of ice-sheet volume. *Nature* 500(7461):190–193. doi:[10.1038/nature12374](https://doi.org/10.1038/nature12374)
- Alder JR, Hostetler SW (in review) Global climate simulations at 3 ka intervals for the last 21,000 years with the GENMOM coupled atmosphere-ocean model *Quaternary Science Reviews*

- Alder JR, Hostetler SW, Pollard D, Schmittner A (2011) Evaluation of a present-day climate simulation with a new coupled atmosphere-ocean model GENMOM. *Geosci Model Dev* 4(1):69–83. doi:[10.5194/gmd-4-69-2011](https://doi.org/10.5194/gmd-4-69-2011)
- Alley RB, Peteet DM, Piette RA Jr, Pierrehumbert RT, Rhines PB, Stocker TF, Tattey LD, Wallace JM, Marotzke J, Nordhaus WD, Overpeck JT (2003) Abrupt climate change. *Science* 299(5615):2005–2010
- Anderson P, Bermike O, Bigelow N, Brigham-Grette J, Duvall M, Edwards M, Frechette B, Funder S, Johnsen S, Knies J, Koerner R, Lozhkin A, Marshall S, Matthiessen J, Macdonald G, Miller G, Montoya M, Muhs D, Otto-Bliesner B, Overpeck J, Reeh N, Sejrup HP, Spielhagen R, Turner C, Velichko A (2006) Last Interglacial Arctic warmth confirms polar amplification of climate change. *Quatern Sci Rev* 25(13–14):1383–1400
- Asmerom Y, Polyak V, Burns S, Rasmussen J (2007) Solar forcing of Holocene climate: New insights from a speleothem record, southwestern United States. *Geology* 35(1):1–4
- Barnosky CW, Anderson PM, Bartlein PJ (1987) The northwestern U.S. during deglaciation: vegetational history and paleoclimatic implications. In: Ruddiman WF, Wright HE, Jr. (eds) North America and adjacent oceans during the last deglaciation, vol K-3. Geological Society of America, Boulder, pp 289–321
- Bartlein PJ (1997) Past environmental changes: characteristic features of Quaternary climate variations. In: Huntley B, Cramer W, Morgan A, Prentice HC, Allen JRM (eds) Past and future rapid environmental change, vol 147., NATO ASI SeriesSpringer, Berlin, pp 11–29
- Bartlein PJ, Hostetler SW (2004) Modeling paleoclimates. In: Gillespie AR, Porter SC, Atwater BF (eds) The Quaternary period in the United States, vol 1., Developments in Quaternary Science, Elsevier, Amsterdam, pp 563–582
- Bartlein PJ, Prentice IC (1989) Orbital variations, climate and paleoecology. *Trends Ecol Evol* 4:195–199
- Bartlein PJ, Whitlock C (1993) Paleoclimatic interpretation of the Elk Lake pollen record. In: Bradbury JP, Dean WE (eds) Elk Lake, Minnesota: evidence for rapid climate change in the north-central United States, vol Special., Paper 276 Geological Society of America, Boulder, pp 275–293
- Bartlein PJ, Anderson KH, Anderson PM, Edwards ME, Mock CJ, Thompson RS, Webb RS, Webb T III, Whitlock C (1998) Paleoclimate simulations for North America over the past 21,000 years: features of the simulated climate and comparisons with paleoenvironmental data. *Quatern Sci Rev* 17(6–7):549–585
- Bartlein PJ, Harrison SP, Brewer S, Connor S, Davis BAS, Gajewski K, Guiot J, Harrison-Prentice TI, Henderson A, Peyron O, Prentice IC, Scholze M, Seppe H, Shuman B, Sugita S, Thompson RS, Viau AE, Williams J, Wu H (2011) Pollen-based continental climate reconstructions at 6 and 21 ka: a global synthesis. *Clim Dyn* 37(3–4):775–802. doi:[10.1007/s00382-010-0904-1](https://doi.org/10.1007/s00382-010-0904-1)
- Beerling DJ, Royer DL (2011) Convergent cenozoic CO<sub>2</sub> history. *Nat Geosci* 4(7):418–420. doi:[10.1038/ngeo1186](https://doi.org/10.1038/ngeo1186)
- Bennett KD (1997) Evolution and ecology: the pace of life. Cambridge studies in ecology. Cambridge University Press, Cambridge
- Berger A (1978) Long-term variations of caloric insolation resulting from the earth's orbital elements. *Quatern Res* 9:139–167
- Berger A, Loutre MF (1991) Insolation values for the climate of the last 10 million years. *Quatern Sci Rev* 10:297–317
- Bond G, Showers W, Chessby M, Lotti R, Almasi P, deMenocal P, Priore P, Cullen H, Hajdas I, Bonani G (1997) A pervasive millennial-scale cycle in North Atlantic Holocene and glacial climates. *Science* 278(14 November):1257–1266
- Bonfils C, de Noblet-Ducoudré N, Guiot J, Bartlein P (2004) Some mechanisms of mid-Holocene climate change in Europe, inferred from comparing PMIP models to data. *Clim Dyn* 23:79–98
- Boslough M, Nicoll K, Holliday V, Daulton TL, Meltzer D, Pinter N, Scott AC, Surovell T, Claeyns P, Gill J, Paquay F, Marlon J, Bartlein P, Whitlock C, Grayson D, Jull AJT (2012) Arguments and evidence against a younger dryas impact event. In: Climates, landscapes, and

- civilizations, vol 198. *Geophys. Monogr. Ser.* AGU, Washington, DC, pp 13–26. doi:[10.1029/2012gm001209](https://doi.org/10.1029/2012gm001209)
- Bothe O, Jungclaus JH, Zanchettin (2013) Consistency of the multi-model CMIP5/PMIP3-past1000 ensemble. *Clim Past* 9:2471–2487. doi: [10.5194/cp-9-2471-2013](https://doi.org/10.5194/cp-9-2471-2013)
- Braconnot P, Harrison SP, Kageyama M, Bartlein PJ, Masson-Delmotte V, Abe-Ouchi A, Otto-Bliesner B, Zhao Y (2012) Evaluation of climate models using palaeoclimatic data. *Nat Clim Chang* 2(6):417–424. doi: [10.1038/Nclimate1456](https://doi.org/10.1038/Nclimate1456)
- Bradley RS (1999) Quaternary paleoclimatology, 2nd edn. Academic Press, San Diego
- Broecker WS, Denton GH, Edwards RL, Cheng H, Alley RB, Putnam AE (2010) Putting the Younger Dryas cold event into context. *Quatern Sci Rev* 29(9–10):1078–1081. doi:[http://dx.doi.org/10.1016/j.quascirev.2010.02.019](https://doi.org/10.1016/j.quascirev.2010.02.019)
- Carlson AE (2010) What caused the Younger Dryas cold event? *Geology* 38(4):383–384. doi: [10.1130/focus042010.1](https://doi.org/10.1130/focus042010.1)
- Carlson AE, Clark PU, Haley BA, Klinkhammer GP, Simmons K, Brook EJ, Meissner KJ (2007) Geochemical proxies of North American freshwater routing during the Younger Dryas cold event. *PNAS* 104(16):6556–6561. doi: [10.1073/pnas.0611313104](https://doi.org/10.1073/pnas.0611313104)
- Charman DJ, Beilman DW, Blaauw M, Booth RK, Brewer S, Chambers FM, Christen JA, Gallego-Sala A, Harrison SP, Hughes PDM, Jackson ST, Korhola A, Mauquoy D, Mitchell FJG, Prentice IC, van der Linden M, De Vleeschouwer F, Yu ZC, Alm J, Bauer IE, Corish YMC, Garneau M, Hohl V, Huang Y, Karofeld E, Le Roux G, Loisel J, Moschen R, Nichols JE, Nieminen TM, MacDonald GM, Phadtare NR, Rausch N, Sillasoo U, Swindles GT, Tuittila ES, Ukonmaanaho L, Valiranta M, van Bellen S, van Geel B, Vitt DH, Zhao Y (2013) Climate-related changes in peatland carbon accumulation during the last millennium. *Biogeosciences* 10(2):929–944. doi: [10.5194/bg-10-929-2013](https://doi.org/10.5194/bg-10-929-2013)
- Cheng H, Edwards RL, Broecker WS, Denton GH, Kong X, Wang Y, Zhang R, Wang X (2009) Ice age terminations. *Science* 326(5950):248–252. doi: [10.1126/science.1177840](https://doi.org/10.1126/science.1177840)
- Clark PU, Dyke AS, Shakun JD, Carlson AE, Clark J, Wohlfarth B, Mitrovica JX, Hostetler SW, McCabe AM (2009) The last glacial maximum. *Science* 325(5941):710–714. doi: [10.1126/science.1172873](https://doi.org/10.1126/science.1172873)
- Clark PU, Shakun JD, Baker PA, Bartlein PJ, Brewer S, Brook E, Carlson AE, Cheng H, Kaufman DS, Liu Z, Marchitto TM, Mix AC, Morrill C, Otto-Bliesner BL, Pahnke K, Russell JM, Whitlock C, Adkins JF, Blois JL, Clark J, Colman SM, Curry WB, Flower BP, He F, Johnson TC, Lynch-Stieglitz J, Markgraf V, McManus J, Mitrovica JX, Moreno PI, Williams JW (2012) Global climate evolution during the last deglaciation. *PNAS*. doi: [10.1073/pnas.1116619109](https://doi.org/10.1073/pnas.1116619109)
- COHMAP Members (1988) Climatic changes of the last 18,000 years: observations and model simulations. *Science* 241:1043–1052
- Committee on Surface Temperature Reconstructions for the Last 2000 Years (2006) Surface temperature reconstructions for the last 2,000 years. The National Academies Press, Washington
- Committee on the Effects of Solar Variability on Earth's Climate (2012) The effects of solar variability on earth's climate: a workshop report. The National Academies Press, Washington
- Condron A, Winsor P (2012) Meltwater routing and the Younger Dryas. *Proc Natl Acad Sci USA* 109(49):19928–19933. doi: [10.1073/pnas.1207381109](https://doi.org/10.1073/pnas.1207381109)
- Cook ER, Woodhouse CA, Eakin CM, Meko DM, Stahle DW (2004) Long-term aridity changes in the western United States. *Science* 306(5698):1015–1018
- Cook ER, P.J. Bartlein, N.S. Diffenbaugh, R. Seager, B.N. Shuman, R.S. Webb, J.W. Williams, C. Woodhouse (2008) Hydrological variability and change. In: Abrupt climate change. A report by the U.S. climate change science program and the subcommittee on global change research. U.S. climate change science program, synthesis and assessment product 3.4. U.S. Geological Survey, Reston VA, pp 143–257
- Cornell SE, Prentice IC, House JI, Downy CJ (2012) Understanding the earth system. Cambridge University Press, Cambridge
- Cronin TM (2010) Paleoclimatology. Columbia University Press, New York

- Diffenbaugh NS, Ashfaq M, Shuman B, Williams JW, Bartlein PJ (2006) Summer aridity in the United States: response to mid-Holocene changes in insolation and sea surface temperature. *Geophys Res Lett* 33:(22)
- Donders T, de Boer H, Finsinger W, Grimm E, Dekker S, Reichart G, Wagner-Cremer F (2011a) Impact of the Atlantic Warm Pool on precipitation and temperature in Florida during North Atlantic cold spells. *Clim Dyn* 36(1):109–118. doi:[10.1007/s00382-009-0702-9](https://doi.org/10.1007/s00382-009-0702-9)
- Donders TH, de Boer HJ, Finsinger W, Grimm EC, Dekker SC, Reichart GJ, Wagner-Cremer F (2011b) Impact of the Atlantic Warm Pool on precipitation and temperature in Florida during North Atlantic cold spells. *Clim Dyn* 36(1–2):109–118. doi:[10.1007/s00382-009-0702-9](https://doi.org/10.1007/s00382-009-0702-9)
- Dyke AS (2004) An outline of North American deglaciation with emphasis on central and northern Canada. In: Ehlers J, Gibbard PL (eds) *Quaternary glaciations—extent and chronology, part II: North America*. Elsevier, Amsterdam, pp 373–424
- Ely L (1997) Response of extreme floods in the southwestern United States to climatic variations in the late Holocene. *Geomorphology* 19:175–201
- Firestone RB, West A, Kennett JP, Becker L, Bunch TE, Revay ZS, Schultz PH, Belgia T, Kennett DJ, Erlandson JM, Dickenson OJ, Goodyear AC, Harris RS, Howard GA, Kloosterman JB, Lechler P, Mayewski PA, Montgomery J, Poreda R, Darrah T, Hee SSQ, Smith AR, Stich A, Topping W, Wittke JH, Wolbach WS (2007) Evidence for an extraterrestrial impact 12,900 years ago that contributed to the megafaunal extinctions and the Younger Dryas cooling. *PNAS* 104(41):16016–16021. doi:[10.1073/pnas.0706977104](https://doi.org/10.1073/pnas.0706977104)
- Forman SL, Oglesby R, Webb RS (2001) Temporal and spatial patterns of Holocene dune activity on the great plains of North America: megadroughts and climate links. *Global Planet Change* 29(1–2):1–29
- Gajewski K, Viau A, Sawada M, Atkinson D, Wilson S (2001) Sphagnum peatland distribution in North America and Eurasia during the past 21,000 years. *Global Biogeochem Cycles* 15(2):297–310
- Gavin DG, Henderson ACG, Westover KS, Fritz SC, Walker IR, Leng MJ, Hu FS (2011) Abrupt Holocene climate change and potential response to solar forcing in western Canada. *Quatern Sci Rev* 30(9–10):1243–1255. doi:[10.1016/j.quascirev.2011.03.003](https://doi.org/10.1016/j.quascirev.2011.03.003)
- Grimm EC, Jacobson GL, Jr., Watts WA, Hansen BCS, Maasch KA (1993) A 50,000-year record of climate oscillations from Florida and its temporal correlation with Heinrich events. *Science* 261(9 July):198–200
- Grootes PM, Stuiver M, White JWC, Johnsen S, Jouzel J (1993) Comparison of oxygen-isotope records from the gisp2 and grip Greenland ice cores. *Nature* 366(6455):552–554
- Harrison SP, Bartlein PJ (2012) Records from the past, lessons for the future: what the palaeorecord implies about mechanisms of global change. In: Henderson-Sellers A, McGuffie KJ (eds) *The future of the world's climate*, 2nd edn. Elsevier, pp 403–476. doi:[10.1016/B978-0-12-386917-3.00014-2](https://doi.org/10.1016/B978-0-12-386917-3.00014-2)
- Harrison SP, Prentice IC, Guiot J (1993) Climatic controls on Holocene lake-level changes in Europe. *Clim Dyn* 8:189–200
- Harrison SP, Kutzbach JE, Liu Z, Bartlein PJ, Otto-Bliesner B, Muhs D, Prentice IC, Thompson RS (2003) Mid-Holocene climates of the Americas: a dynamical response to changed seasonality. *Clim Dyn* 20(7–8):663–688
- Harrison SP, Bartlein PJ, Brewer S, Prentice IC, Boyd M, Hessler I, Holmgren K, Izumi K, Willis K (2013) Climate model benchmarking with glacial and mid-Holocene climates. *Clim Dyn* 40:951–962
- Haug GH, Tiedemann R (1998) Effect of the formation of the Isthmus of Panama on Atlantic Ocean thermohaline circulation. *Nature* 393(18 June):673–676
- Haug GH, Ganopolski A, Sigman DM, Rosell-Mele A, Swann GEA, Tiedemann R, Jaccard SL, Bollmann J, Maslin MA, Leng MJ, Eglinton G (2005) North Pacific seasonality and the glaciation of North America 2.7 million years ago. *Nature* 433(7028):821
- Hegerl GC, Zwiers FW, Braconnot P, Gillett NP, Luo Y, Marengo Orsini JA, Nicholls N, Penner JE, Stott PA (2007) Understanding and attributing climate change. In: Solomon S, Qin D, Manning M et al. (eds) *Climate change 2007*

- Hendy I, Kennett J (2003) Tropical forcing of North Pacific intermediate water distribution during late Quaternary rapid climate change? *Quatern Sci Rev* 22(5–7):673–689
- Hendy I, Kennett J, Roark E, Ingram B (2002) Apparent synchronicity of submillennial scale climate events between Greenland and Santa Barbara Basin, California from 30–10 ka. *Quatern Sci Rev* 21(10):1167–1184
- Hu F, Kaufman D, Yoneji S, Nelson D, Shemesh A, Huang Y, Tian J, Bond G, Clegg B, Brown T (2003) Cyclic variation and solar forcing of Holocene climate in the Alaskan subarctic. *Science* 301(5641):1890–1893
- Imbrie J, Boyle EA, Clemens SC, Duffy A, Howard WR, Kukla G, Kutzbach JE, Martinson DG, McIntyre A, Mix AC, Molino B, Morley JJ, Peterson LC, Pisias NG, Prell WL, Raymo ME, Shackleton NJ, Toggweiler JR (1992) On the structure and origin of major glaciation cycles, 1. linear responses to Milankovitch forcing. *Paleoceanography* 7:701–738
- IPCC (ed) (2007) Climate Change 2007: the physical science basis. Contribution of working group I to the fourth assessment report of the intergovernmental panel on climate change. Cambridge University Press, Cambridge United Kingdom and New York
- Izumi K, Bartlein PJ, Harrison SP (2013) Consistent large-scale temperature responses in warm and cold climates. *Geophys Res Lett* 40(9):1817–1823. doi:[10.1002/grl.50350](https://doi.org/10.1002/grl.50350)
- Jimenez-Moreno G, Anderson RS, Fawcett PJ (2007) Orbital- and millennial-scale vegetation and climate changes of the past 225 ka from Bear Lake, Utah–Idaho (USA). *Quatern Sci Rev* 26(13–14):1713–1724. doi:[10.1016/j.quascirev.2007.05.001](https://doi.org/10.1016/j.quascirev.2007.05.001)
- Jiménez-Moreno G, Fawcett PJ, Scott Anderson R (2008) Millennial- and centennial-scale vegetation and climate changes during the late Pleistocene and Holocene from northern New Mexico (USA). *Quatern Sci Rev* 27(13–14):1442–1452. doi:<http://dx.doi.org/10.1016/j.quascirev.2008.04.004>
- Jiménez-Moreno G, Anderson RS, Desprat S, Grigg LD, Grimm EC, Heusser LE, Jacobs BF, López-Martínez C, Whitlock CL, Willard DA (2010) Millennial-scale variability during the last glacial in vegetation records from North America. *Quatern Sci Rev* 29(21–22): 2865–2881. doi:<http://dx.doi.org/10.1016/j.quascirev.2009.12.013>
- Jungclaus JH, Lorenz SJ, Timmreck C, Reick CH, Brovkin V, Six K, Segschneider J, Giorgetta MA, Crowley TJ, Pongratz J, Krivova NA, Vieira LE, Solanki SK, Klocke D, Botzet M, Esch M, Gayler V, Haak H, Radatz TJ, Roeckner E, Schnur R, Widmann H, Claussen M, Stevens B, Marotzke J (2010) Climate and carbon-cycle variability over the last millennium. *Clim Past* 6(5):723–737. doi:[10.5194/cp-6-723-2010](https://doi.org/10.5194/cp-6-723-2010)
- Kaufman DS, Schneider DP, McKay NP, Ammann CM, Bradley RS, Briffa KR, Miller GH, Otto-Btiesner BL, Overpeck JT, Vinther BM, Arctic Lakes 2k Project Members (2009) Recent warming reverses long-term arctic cooling. *Science* 325(5945):1236–1239. doi:[10.1126/science.1173983](https://doi.org/10.1126/science.1173983)
- Kaufman DS, Ager TA, Anderson NJ, Anderson PM, Andrews JT, Bartlein PJ, Brubaker LB, Coats LL, Cwynar LC, Duvall ML, Dyke AS, Edwards ME, Eisner WR, Gajewski K, Geirsdottir A, Hu FS, Jennings AE, Kaplan MR, Kerwin MN, Lozhkin AV, MacDonald GM, Miller GH, Mock CJ, Oswald WW, Otto-Btiesner BL, Porinchu DF, Ruhland K, Smol JP, Steig EJ, Wolfe BB (2004) Holocene thermal maximum in the western Arctic (0–180 degrees W). *Quatern Sci Rev* 23(5–6):529–560. doi:[10.1016/j.quascirev.2003.09.007](https://doi.org/10.1016/j.quascirev.2003.09.007)
- Knox JC (1993) Large increases in flood magnitude in response to modest changes in climate. *Nature* 361(4 February):430–432
- Knox JC (2000) Sensitivity of modern and Holocene floods to climate change. *Quatern Sci Rev* 19:439–457
- Kohler P, Bintanja R, Fischer H, Joos F, Knutti R, Lohmann G, Masson-Delmotte V (2010) What caused earth's temperature variations during the last 800,000 years? Data-based evidence on radiative forcing and constraints on climate sensitivity. *Quatern Sci Rev* 29(1–2):129–145. doi:[10.1016/j.quascirev.2009.09.026](https://doi.org/10.1016/j.quascirev.2009.09.026)
- Kutzbach JE, Guetter PJ (1986) The influence of changing orbital patterns and surface boundary conditions on climate simulations for the past 18,000 years. *J Atmos Sci* 43:1726–1759

- Kutzbach JE, Bartlein PJ, Prentice IC, Ruddiman WF, Street-Perrott FA, Webb T III, Wright HE Jr (1993) Epilogue. In: Wright HE Jr, Kutzbach JE, Webb T III, Ruddiman WF, Street-Perrott FA, Bartlein PJ (eds) Global climates since the last glacial maximum, vol 20., UnivMinnesota Press, Minneapolis, pp 536–542
- Landrum L, Otto-Bliesner BL, Wahl ER, Conley A, Lawrence P, Rosenbloom N, Teng H (2013) Last Millennium climate and its variability in CCSM4. *J Clim*, 26:1085–1111. doi: [10.1175/JCLI-D-11-00326.1](https://doi.org/10.1175/JCLI-D-11-00326.1)
- Lawrence KT, Liu ZH, Herbert TD (2006) Evolution of the eastern tropical Pacific through Plio-Pleistocene glaciation. *Science* 312(5770):79–83. doi: [10.1126/science.1120395](https://doi.org/10.1126/science.1120395)
- Li G, Harrison SP, Bartlein PJ, Izumi K, Prentice IC (2013) Precipitation scaling with temperature in warm and cold climates: an analysis of CMIP5 simulations. *Geophys Res Lett* :n/a-n/a. doi: [10.1002/grl.50730](https://doi.org/10.1002/grl.50730)
- Lisiecki LE, Raymo ME (2005) A Pliocene-Pleistocene stack of 57 globally distributed benthic delta O-18 records. *Paleoceanography* 20(1)
- Liu Z, Harrison S, Kutzbach J, Otto-Bliesner B (2004) Global monsoons in the mid-Holocene and oceanic feedback. *Clim Dyn* 22(2–3):157–182
- Liu Z, Otto-Bliesner BL, He F, Brady EC, Tomas R, Clark PU, Carlson AE, Lynch-Stieglitz J, Curry W, Brook E, Erickson D, Jacob R, Kutzbach J, Cheng J (2009) Transient simulation of last deglaciation with a new mechanism for Bolling-Allerod warming. *Science* 325(5938):310–314. doi: [10.1126/science.1171041](https://doi.org/10.1126/science.1171041)
- Liu Z, Carlson AE, He F, Brady EC, Otto-Bliesner BL, Briegleb BP, Wehrenberg M, Clark PU, Wu S, Cheng J, Zhang J, Noone D, Zhu J (2012) Younger Dryas cooling and the Greenland climate response to CO<sub>2</sub>. *PNAS* 109(28):11101–11104. doi: [10.1073/pnas.1202183109](https://doi.org/10.1073/pnas.1202183109)
- Mann ME, Zhang ZH, Hughes MK, Bradley RS, Miller SK, Rutherford S, Ni FB (2008) Proxy-based reconstructions of hemispheric and global surface temperature variations over the past two millennia. *Proc Natl Acad Sci USA* 105(36):13252–13257. doi: [10.1073/pnas.0805721105](https://doi.org/10.1073/pnas.0805721105)
- Mann ME, Zhang ZH, Rutherford S, Bradley RS, Hughes MK, Shindell D, Ammann C, Faluvegi G, Ni FB (2009) Global signatures and dynamical origins of the little ice age and medieval climate anomaly. *Science* 326(5957):1256–1260. doi: [10.1126/science.1177303](https://doi.org/10.1126/science.1177303)
- Marcott SA, Shakun JD, Clark PU, Mix AC (2013) A reconstruction of regional and global temperature for the past 11,300 years. *Science* 339(6124):1198–1201. doi: [10.1126/science.1228026](https://doi.org/10.1126/science.1228026)
- Marlon JR, Bartlein PJ, Walsh MK, Harrison SP, Brown KJ, Edwards ME, Higuera PE, Power MJ, Anderson RS, Briles C, Brunelle A, Carcaillet C, Daniels M, Hu FS, Lavoie M, Long C, Minckley T, Richard PJH, Scott AC, Shafer DS, Tinner W, Umbanhowar Jr. CE, Whitlock C (2009) Wildfire responses to abrupt climate change in North America. *PNAS*. doi: [doi:10.1073/pnas.0808212106](https://doi.org/10.1073/pnas.0808212106)
- Martinson DG, Pisias NG, Hays JD, Imbrie J, Moore TC Jr, Shackleton NJ (1987) Age dating and the orbital theory of the ice ages: development of a high-resolution 0 to 300,000-year chronostratigraphy. *Quatern Res* 27:1–29
- Martrat B, Grimalt JO, Shackleton NJ, de Abreu L, Hutterli MA, Stocker TF (2007) Four climate cycles of recurring deep and surface water destabilizations on the Iberian margin. *Science* 317(5837):502–507. doi: [10.1126/science.1139994](https://doi.org/10.1126/science.1139994)
- Miao XD, Mason JA, Swinehart JB, Loope DB, Hanson PR, Goble RJ, Liu XD (2007) A 10,000 year record of dune activity, dust storms, and severe drought in the central great plains. *Geology* 35(2):119–122
- Mock C, Bartlein P (1995) Spatial variability of late-quaternary paleoclimates in the western United States. *Quatern Res* 44(3):425–433
- Mock CJ, Brunelle-Daines AR (1999) A modern analogue of western United States summer palaeoclimate at 6000 years before present. *Holocene* 9(5):541–545
- North Greenland Ice Core Project Members (2004) High resolution climate record of the Northern Hemisphere reaching into the last glacial Interglacial period. *Nature* 431:147–151
- Overpeck JT, Alley RB, Kiehl JT, Otto-Bliesner BL, Miller GH, Muhs DR (2006) Paleoclimatic evidence for future ice-sheet instability and rapid sea-level rise. *Science* 311(5768):1747–1750

- PAGES 2k Consortium (2013) Continental-scale temperature variability during the past two millennia. *Nat Geosci* 6(5):339–346. doi:[10.1038/ngeo1797](https://doi.org/10.1038/ngeo1797)
- Peltier WR (2004) Global glacial isostasy and the surface of the ice-age earth: The ice-5G (VM2) model and grace. *Annu Rev Earth Planet Sci* 32:111–149. doi:[10.1146/annurev.earth.32.082503.144359](https://doi.org/10.1146/annurev.earth.32.082503.144359)
- Pixeot JP, Oort AH (1992) Physics of climate. American Institute of Physics, New York
- Pinter N, Scott AC, Daulton TL, Podoll A, Koeberl C, Anderson RS, Ishman SE (2011) The Younger Dryas impact hypothesis: A requiem. *Earth-Sci Rev* 106 (3–4):247–264. doi:<http://dx.doi.org/10.1016/j.earscirev.2011.02.005>
- Forster P, Ramaswamy V, Artaxo P, Berntsen T, Betts R, Fahey DW, Haywood J, Lean J, Lowe DC, Myhre G, Nganga J, Prinn R, Raga G, M. S, Dorland R (2007) Changes in atmospheric constituents and in radiative forcing. In: Solomon S, Qin D, Manning M et al. (eds) *Climate change 2007*
- Ruddiman WF (2006) Orbital changes and climate. *Quatern Sci Rev* 25(23–24):3092–3112
- Saltzman B (2002) *Dynamical paleoclimatology: generalized theory of global climate change*. Academic Press, San Diego
- Sanchez Goñi MF, Harrison SP (2010) Millennial-scale climate variability and vegetation changes during the last glacial: concepts and terminology. *Quatern Sci Rev* 29(21–22):2823–2827. doi:<http://dx.doi.org/10.1016/j.quascirev.2009.11.014>
- Schmidt M, Spero H, Lea D (2004) Links between salinity variation in the Caribbean and North Atlantic thermohaline circulation. *Nature* 428(6979):160–163
- Schmidt GA, Jungclaus JH, Ammann CM, Bard E, Braconnot P, Crowley TJ, Delaygue G, Joos F, Krivova NA, Muscheler R, Otto-Bliesner BL, Pongratz J, Shindell DT, Solanki SK, Steinhilber F, Vieira LEA (2011) Climate forcing reconstructions for use in PMIP simulations of the last millennium (v1.0). *Geosci Model Dev* 4(1):33–45. doi:[10.5194/gmd-4-33-2011](https://doi.org/10.5194/gmd-4-33-2011)
- Shinker JJ, Bartlein PJ, Shuman B (2006) Synoptic and dynamic climate controls of North American mid-continental aridity. *Quatern Sci Rev* 25:1401–1417
- Shuman BN (2012) Patterns, processes, and impacts of abrupt climate change in a warm world: the past 11,700 years. *Wiley Interdisc Rev: Clim Change* 3(1):19–43. doi:[10.1002/wcc.152](https://doi.org/10.1002/wcc.152)
- Shuman B, Plank C (2011) Orbital, ice sheet, and possible solar controls on Holocene moisture trends in the North Atlantic drainage basin. *Geology* 39(2):151–154. doi:[10.1130/g31387.1](https://doi.org/10.1130/g31387.1)
- Shuman B, Webb T III, Bartlein PJ, Williams JW (2002) The anatomy of a climatic oscillation: vegetation change in eastern North America during the Younger Dryas chronozone. *Quatern Sci Rev* 21:1763–1916
- Steffen W, Persson A, Deutsch L, Zalasiewicz J, Williams M, Richardson K, Crumley C, Crutzen P, Folke C, Gordon L, Molina M, Ramanathan V, Rockstrom J, Scheffer M, Schellnhuber HJ, Svedin U (2011) The anthropocene: from global change to planetary stewardship. *Ambio* 40(7):739–761. doi:[10.1007/s13280-011-0185-x](https://doi.org/10.1007/s13280-011-0185-x)
- Steffensen JP, Andersen KK, Bigler M, Clausen HB, Dahl-Jensen D, Fischer H, Goto-Azuma K, Hansson M, Johnsen SJ, Jouzel J, Masson-Delmotte V, Popp T, Rasmussen SO, Rothlisberger R, Ruth U, Stauffer B, Siggaard-Andersen ML, Sveinbjornsdottir AE, Svensson A, White JWC (2008) High-resolution Greenland ice core data show abrupt climate change happens in few years. *Science* 321(5889):680–684. doi:[10.1126/science.1157707](https://doi.org/10.1126/science.1157707)
- Stuiver M, Grootes PM, Braziunas TF (1995) The GISP2  $\delta^{18}\text{O}$  climate record of the past 16,500 years and the role of the Sun, ocean, and volcanoes. *Quatern Res* 44(3):341–354
- Teller JT (2012) Importance of freshwater injections into the Arctic Ocean in triggering the Younger Dryas cooling. *Proc Natl Acad Sci USA* 109(49):19880–19881. doi:[10.1073/pnas.1218344109](https://doi.org/10.1073/pnas.1218344109)
- Thompson RS, Whitlock C, Bartlein PJ, Harrison SP, Spaulding WG (1993) Climatic changes in western United States since 18,000 yr B.P. In: Wright HE Jr, Kutzbach JE, Webb T III, Ruddiman WF, Street-Perrott FA, Bartlein PJ (eds) *Global climates since the last glacial maximum*, vol 18. University of Minnesota Press, Minneapolis, pp 468–513
- Viau AE, Gajewski K, Sawada MC, Fines P (2006) Millennial-scale temperature variations in North America during the Holocene. *J Geophys Res D: Atmos* 111:Article Number D09102

- Webb T III, Bartlein PJ (1992) Global changes during the last 3 million years: climatic controls and biotic responses. *Annu Rev Ecol Syst* 23:141–173
- Webb T III, Cushing EJ, Wright HE Jr (1983) Holocene changes in the vegetation of the Midwest. In: Wright HE Jr (ed) Late-quaternary environments of the United States, vol 2., UnivMinnesota Press, Minneapolis, pp 142–165
- Webb T III, Bartlein PJ, Kutzbach JE (1987) Climatic change in eastern North America during the past 18,000 Years: comparisons of pollen data with model results. In: Ruddiman WF, Wright HE Jr (eds) North America and adjacent oceans during the last deglaciation, vol K-3. Geological Society of America, Boulder, pp 447–462
- Webb T III, Bartlein PJ, Harrison SP, Anderson KH (1993) Vegetation, lake levels, and climate in eastern North America for the past 18,000 years. In: Wright HE Jr, Kutzbach JE, Webb T III, Ruddiman WF, Street-Perrott FA, Bartlein PJ (eds) Global climates since the last glacial maximum, vol 17. University of Minnesota Press, Minneapolis, pp 415–467
- Webb T III, Anderson KH, Bartlein PJ, Webb RS (1998) Late Quaternary climate change in eastern North America: a comparison of pollen-derived estimates with climate model results. *Quatern Sci Rev* 17(6–7):587–606
- Whitlock C, Bartlein PJ (1997) Vegetation and climate change in northwest America during the past 125 kyr. *Nature* 388(6637):57–61
- Williams JW (2002) Variations in tree cover in North America since the last glacial maximum. *Global Planet Change* 35:1–23
- Williams JW, Shuman BN, Webb T III, Bartlein PJ, Leduc PL (2004) Late-quaternary vegetation dynamics in North America: scaling from taxa to biomes. *Ecol Monogr* 74(2):309–334
- Williams JW, Shuman BN, Bartlein PJ (2009) Abrupt responses of the prairie-forest ecotone to early Holocene aridity in mid-continent North America. *Global Planet Change* 66:195–207
- Williams JW, Shuman B, Bartlein PJ, Diffenbaugh NS, Webb T (2010) Rapid, time-transgressive, and variable responses to early Holocene midcontinental drying in North America. *Geology* 38(2):135–138. doi:[10.1130/G30413.1](https://doi.org/10.1130/G30413.1)
- Wolff EW, Chappellaz J, Blunier T, Rasmussen SO, Svensson A (2010) Millennial-scale variability during the last glacial: the ice core record. *Quatern Sci Rev* 29(21–22):2828–2838. doi:<http://dx.doi.org/10.1016/j.quascirev.2009.10.013>
- Wolff E, Harrison SP, Knutti R, Sanchez-Goni MF, Wild O, Daniau AL, Masson-Delmotte V, Prentice IC, Spahni R (2012) How has climate responded to natural perturbations? In: Cornell SE, Prentice IC, House JI, Downy CJ (eds) Understanding the earth system. Cambridge University Press, Cambridge, pp 72–101
- Wright HE, Hu FS, Stefanova I, Tian J, Brown TA (2004) A chronological framework for the Holocene vegetational history of central Minnesota: the steel lake pollen record. *Quatern Sci Rev* 23(5–6):611–626
- Yu ZC (2012) Northern peatland carbon stocks and dynamics: a review. *Biogeosciences* 9(10):4071–4085. doi:[10.5194/bg-9-4071-2012](https://doi.org/10.5194/bg-9-4071-2012)
- Zachos J, Pagani H, Sloan L, Thomas E, Billups K (2001) Trends, rhythms, and aberrations in global climate 65 Ma to present. *Science* 292(5517):686–693